BNWL-371 PT2
UC-80 Reactor Technology

CROSSFLOW MIXING BETWEEN PARALLEL FLOW CHANNELS DURING BOILING
PART II
MEASUREMENT OF FLOW AND ENTHALPY IN TWO PARALLEL CHANNELS

By

D. S. Rowe and C. W. Angle

Reactor Engineering Section
Engineering Development Department

December 1967

PACIFIC NORTHWEST LABORATORY
RICHLAND, WASHINGTON

This document is furnished pursuant to the Memorandum of Understanding of June 7, 1960, between the U.S. and Canadian Governments, establishing a cooperative program on the development of heavy water moderated power reactors.

Printed in the United States of America
Available from
Clearinghouse for Federal Scientific and Technical Information
National Bureau of Standards, U.S. Department of Commerce
Springfield, Virginia 22151
Price: Printed Copy $3.00; Microfiche $0.65

CROSSFLOW MIXING BETWEEN PARALLEL FLOW CHANNELS DURING BOILING
PART II
MEASUREMENT OF FLOW AND ENTHALPY IN TWO PARALLEL CHANNELS

D. S. Rowe and C. W. Angle

ABSTRACT

Laboratory Experiments were conducted to determine the amount of mixing that occurs between two interconnected flow channels during boiling. The experiments were performed with water at 900 psia flowing through electrically heated test sections that simulated two adjacent channels typical of a 19-rod bundle. The results of the experiments showed that mixing during nonboiling conditions was nearly independent of rod spacing and could be correlated as a function of Reynolds Number. The results also showed that mixing during boiling is not necessarily higher than during nonboiling conditions. Mixing during boiling was found to be dependent upon rod spacing, flow rate, and, possibly, steam quality. The results also agreed well with predictions of the computer program COBRA which was developed in the first part of this study to compute flow, enthalpy and pressure in rod bundle subchannels.

TABLE OF CONTENTS

ABSTRACT iii
LIST OF FIGURES. v
INTRODUCTION 1
SUMMARY AND CONCLUSIONS. 2
EXPERIMENTAL METHOD. 4
Description of Facilities. 4
Test Section Description 6
Instrumentation 8
Test Procedure 9
Method of Data Reduction 10
RESULTS. 12
Subchannel Exit Enthalpy 12
Subchannel Exit Flow 25
Axial Pressure Drop 25
Transverse Pressure Drop 25
Observations During Experiments 28
DISCUSSION 31
Single-Phase Mixing 33
Two-Phase Mixing 37
Pressure Drop. 39
Subchannel Flow Rates. 40
Transverse Cross Flow Resistance 41
Interfacial Shear. 42
ACKNOWLEDGEMENTS 43
REFERENCES 43
NOMENCLATURE 45
APPENDIX A-ERROR ANALYSIS A-1
APPENDIX B-TABULATION OF EXPERIMENTAL DATA B-1
DISTRIBUTION C-1

LIST OF FIGURES

1	System Flow Diagram	5
2	Cross Section View of Assembled Test Section	7
3	Cross Section of Inlet and Outlet Transition and Electrical Connection	7
4	Subchannel Cross Section Dimensions for 0.084 and 0.020 in. Simulated Rod Spacing	13
5	Subchannel Enthalpy Rise and Exit Flow Rate at G = 1.0 x 10^6 lb/hr-ft^2 and 0.084 in. Spacing	14
6	Subchannel Enthalpy Rise and Exit Flow Rate at G = 2.0 x 10^6 lb/hr-ft^2 and 0.084 in. Spacing	15
7	Subchannel Enthalpy Rise and Exit Flow Rate at G = 3.0 x 10^6 lb/hr-ft^2 and 0.084 in. Spacing	16
8	Subchannel Enthalpy Rise and Exit Flow Rate at G = 1.0 x 10^6 lb/hr-ft^2 and 0.020 in. Spacing	17
9	Subchannel Enthalpy Rise and Exit Flow Rate at G = 2.0 x 10^6 lb/hr-ft^2 and 0.020 in. Spacing	18
10	Subchannel Enthalpy Rise and Exit Flow Rate at G = 3.0 x 10^6 lb/hr-ft^2 and 0.020 in. Spacing	19
11	Subchannel Enthalpy Rise and Exit Flow Rate at G = 1.0 x 10^6 lb/hr-ft^2 and 0.084 in. Spacing	20
12	Subchannel Enthalpy Rise and Exit Flow Rate at G = 2.0 x 10^6 lb/hr-ft^2 and 0.084 in. Spacing	21
13	Subchannel Enthalpy Rise and Exit Flow Rate at G = 3.0 x 10^6 lb/hr-ft^2 and 0.084 in. Spacing	22
14	Subchannel Enthalpy Rise and Exit Flow Rate at G = 2.0 x 10^6 lb/hr-ft^2 and 0.020 in. Spacing	23
15	Subchannel Enthalpy Rise and Exit Flow Rate at G = 3.0 x 10^6 lb/hr-ft^2 and 0.020 in. Spacing	24
16	Test Section Pressure Drop During Boiling with 0.084 in. Spacing	26
17	Test Section Pressure Drop During Boiling with 0.020 in. Spacing	27
18	Cold Water Hydraulic Test Results to Determine Flow Split Sensitivity	31

CROSSFLOW MIXING BETWEEN PARALLEL FLOW CHANNELS DURING BOILING
PART II
MEASUREMENT OF FLOW AND ENTHALPY IN TWO PARALLEL CHANNELS

By

D. S. Rowe and C. W. Angle

INTRODUCTION

The purpose of this report is to present the results of laboratory experiments that were performed to determine the amount of natural mixing occurring between two interconnected parallel channels during boiling. These experiments were conducted as the second part of study of two-phase flow and mixing in rod bundle fuel elements under the sponsorship of a cooperative program between the United States and Canada for the development of heavy water moderated power reactors. The overall purpose of this study is to provide a more accurate means of predicting flow and enthalpy in rod bundle subchannels, thus allowing a more accurate means of correlating conditions under which boiling burnout occurs in rod bundle fuel elements.

In the first part of this study[1] an analytical model and digital computer program, COBRA, was developed to compute the flow, enthalpy and pressure in the subchannels of rod bundle fuel elements during boiling. The mathematical model used to develop COBRA assumed that two mechanisms are simultaneously involved in the mass energy and momentum transport between adjacent rod bundle subchannels. The first mechanism is a diversion crossflow caused by flow redistribution resulting from different pressure distribution in the adjacent subchannels. The second mechanism is a turbulent crossflow caused by the random travel of coolant between adjacent subchannels. The first type of crossflow can be computed fairly well from the equations of the mathematical model; however, the turbulent crossflow cannot – it must be determined from

experiments. Successful application of COBRA to rod bundle subchannel analysis must, therefore, rely on experimentally determined values of turbulent crossflow during both boiling and nonboiling conditions. At the present time only a limited amount of data exists for mixing during nonboiling conditions in rod bundles. For boiling conditions no known data exists. It is essential that mixing during boiling be known before accurate subchannel analyses can be made, thus allowing a more accurate determination of the possible occurrence of boiling burnout.

SUMMARY AND CONCLUSIONS

Laboratory experiments were performed to determine the amount of natural turbulent mixing that occurs between two interconnected parallel channels typical of those in rod bundle nuclear fuel elements. An electrically heated test section which simulates channels formed by rods on a square pitch array located next to rods on a triangular pitch array, was used for the experiments.

All experiments were done with water at 900 psia. Inlet temperatures of 330 °F and 510 °F were considered for nonboiling and boiling experiments, respectively. Mass flow rates of 1, 2, and 3 x 10^6 lb/hr-ft^2, and heat fluxes up to about two-thirds the expected burnout heat flux were considered for simulated rod spacings of 0.020 and 0.084 in.

The amount of natural turbulent mixing was determined by comparing the values of enthalpy at the exit of the test section to the results of calculations using COBRA. The results of the calculations showed that turbulent mixing during nonboiling conditions was nearly independent of rod spacing. A correlation of this data, as a function of Reynolds Number, was made and gave excellent agreement with the experimental results.

Average turbulent mixing during boiling was found to improve by about twice for the 0.084 in. spacing; however, no significant improvement was found for the 0.020 in. spacing. The subchannel exit enthalpy data did not permit local values of mixing during boiling to be determined, but some definite trends existed. Mixing during boiling was not uniform with steam quality. The data indicated that mixing reached a peak at low quality and then decreased at high quality. This effect was most significant for the 0.084 in. spacing.

The conclusions that can be made from these experiments are:

- The digital computer program, COBRA, properly predicts the subchannel conditions of the experiments. By using experimental data such as the type generated in these experiments, COBRA is a valid analytical tool for rod bundle subchannel analysis.
- Natural turbulent mixing during single phase flow is not proportional to rod spacing. A correlation of the experimental data showed that turbulent crossflow per unit length is independent of rod spacing and is nearly proportional to hydraulic diameter and mass velocity. The correlation of the subcooled mixing data is significant since it is the lower limit of mixing in actual rod bundles. Actual rod bundles have higher levels of mixing than predicted from these experiments because of rod spacing devices such as grids, warts, or wire wraps.
- Boiling can cause an increase in mixing for only certain conditions. The experiments show that mixing does not improve significantly for closely spaced rods and that poor mixing could occur at high quality.

EXPERIMENTAL METHOD

DESCRIPTION OF FACILITIES

The experiments were conducted in the Pacific Northwest Laboratory's Low Pressure Heat Transfer Facility[2] which is a closed loop facility nominally rated at a system pressure of 1000 psia with flow rates up to 250 gpm. Slight modification of the facility was required to carry out the experiments (Figure 1). This included the addition of two heat exchangers and various piping and valves to allow separation of the flow streams entering and leaving the test section.

Cold water was pumped through a stream preheater with an outlet temperature of about 200 °F and then through an electric preheater for final adjustment of temperature for the test condition. The flow was then split into two streams prior to entering the bottom of the vertically mounted test section. Valves in the two streams were used to adjust the flow split. When the two separated streams entered the electrically heated test section, they were allowed to mix across the gap between the two flow channels. At the end of the heated section the flow streams were again separated and each entered a "hairpin" heat exchanger where they were condensed and cooled by parallel flow* cooling water at 500 psia.** Valves in each of the cooled streams were used to adjust the exit flow split from the test section. After the streams were combined they passed through the throttle valve that provided system back pressure. The

---

* *Counterflow was initially used but gave oscillating coolant outlet temperatures.*

** *Pressurization was also required to help eliminate oscillations in the cooling outlet temperature caused by film boiling on the cooling side.*

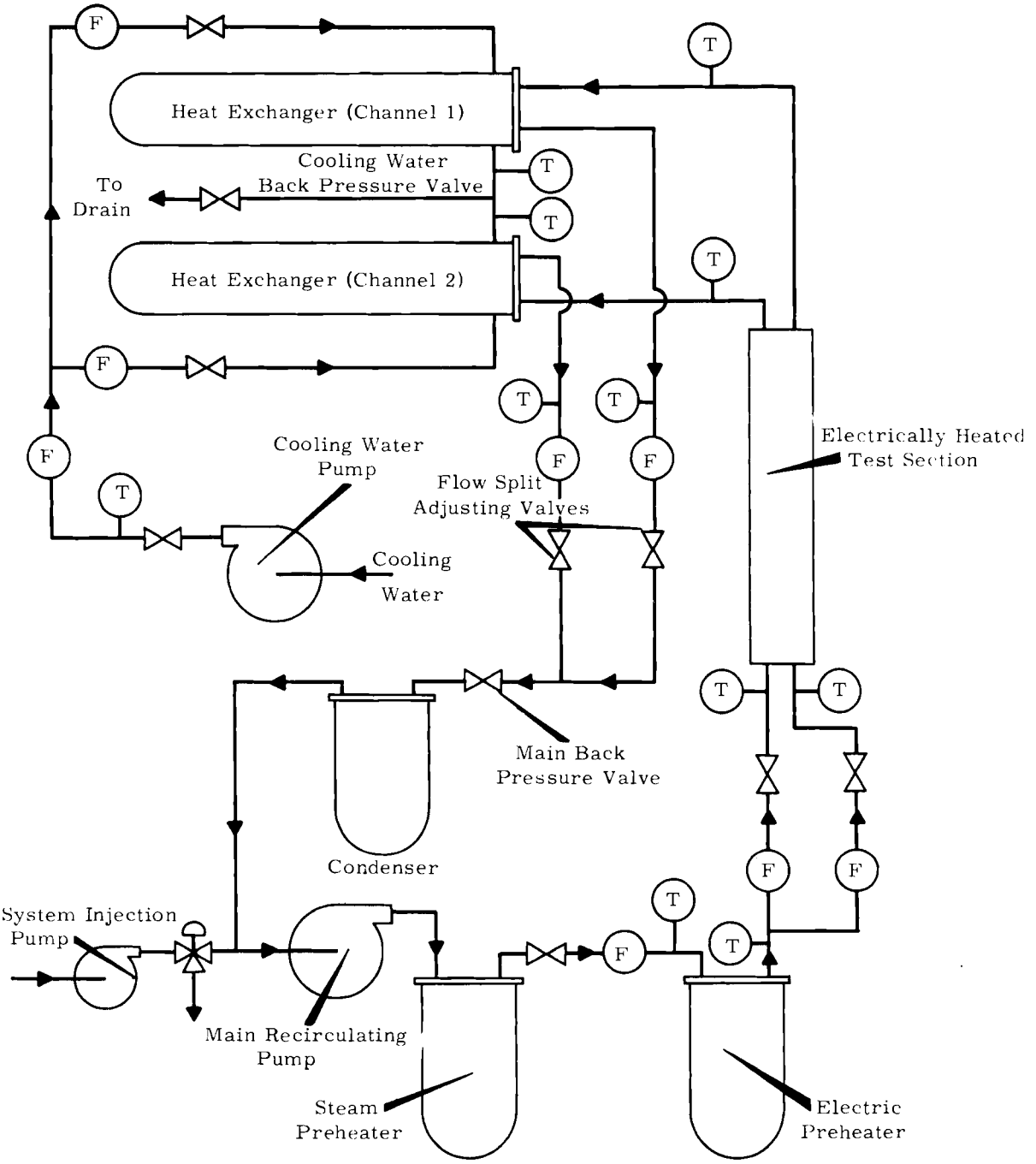

FIGURE 1. System Flow Diagram

main recirculating pump was used simultaneously with this valve to provide the system pressure of 900 psia because the pump has a head of about 1000 psia at low flow rates. After passing through the throttle valve the flow was further cooled by the loop's main condenser and passed on to the suction side of the main recirculating pump. System pressure was controlled by the use of an injection pump with a "feed-bleed" valve at the suction of the main pump.

TEST SECTION DESCRIPTION

The electrically heated test section used for these experiments was constructed from 321 SS tubing with 0.563 in. OD and 0.094 in. wall thickness. The tubing was cut lengthwise and the edges formed as shown in Figure 2. The prepared tube segments were then clamped to a machined copper chill block that provided the proper cross sectional shape and provided a heat sink during welding. Welding of the longitudinal seams was done in a lathe bed with a small "heli-arc" torch supported by the tool holder on the lathe carriage. After small tack welds were made, long segments of continuous weld were made using a selected carriage feed. The welded test section was very straight when it was removed from the copper chill block and required no further work other than preparing the ends for the electrical connections and attachment of instrumentation.

The electrical connections that were brazed to the ends of the heated section also provided the entrance and exit flow separators (Figure 3). These flow separators had about the same flow area and shape as the heated section except for a thin web to separate the two subchannels. The web started 1/2 in. from the ends of the heated section. The 12 in. long inlet piece also provided a transition from the inlet pipes to reduce the turbulence induced from the change in flow area and cross-sectional shape.

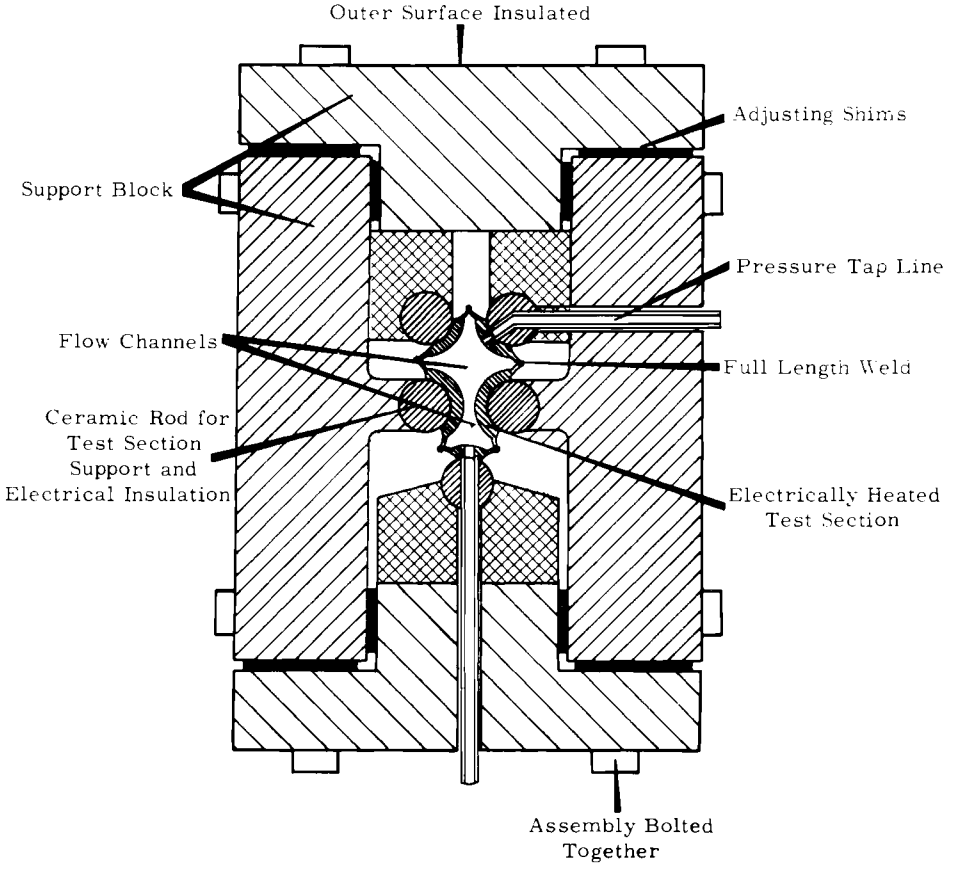

FIGURE 2. Cross Section View of Assembled Test Section

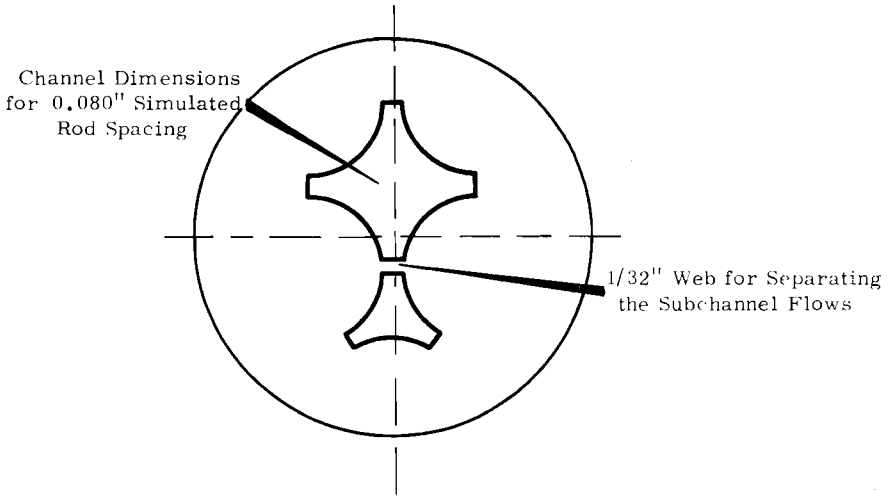

FIGURE 3. Cross Section of Inlet and Outlet Transition and Electrical Connection

The shape of the heated section was maintained by steel support blocks and ceramic ("Mullite") rod segments (Figure 2). Adjustment of the subchannel flow area and gap between the simulated rods was with shims. With the excellent dimensional uniformity of the support blocks and ceramic rod segments, it is estimated that the gap variations were less than about ±0.0015 in. In addition to supporting the test section, the ceramic rod segments electrically insulated the test section from the supporting structure. The low thermal conductivity of the ceramic also helped to thermally insulate the heated section; however, the primary insulation was provided by a 2 in. layer of magnesia around the entire assembly.

Instrumentation

Water temperature was measured with Inconel sheathed, Iron-Constantan thermocouples. They were positioned in the center of the flow stream by an assembly that screwed into a "weldolet" on the pipe wall. The assembly consisted of the sheathed thermocouple brazed inside a small diameter tube, with the tip protruding about 1/4 in., and the tube then brazed into a threaded plug to properly position the thermocouple.

Millivolt output was recorded on automatic digital readout equipment that typed the millivolt reading and punched paper tape for data processing. Actual water temperatures were also continuously recorded on strip chart recorders for a visual account of temperatures during the tests. An ice bath was used to maintain the thermocouple cold junction at 32 °F.

Four Resistance Temperature Detectors (RTD) provided additional temperature measurement and also provided a basis for calibration of the thermocouples. With the low fluid velocities encountered for some experimental conditions, RTD errors were encountered; therefore, they were used for thermocouple calibration at the higher flow rates and the thermocouples data were used for all data reduction.

Potter and Fisher-Porter turbine flow meters were used for all flow measurement. Calibration prior to running the experiments, and at intervals during the experiments, incdicated errors less than about 1%. A few exceptions to this were encountered and will be mentioned later in this report.

Pressure taps were placed on the test section to measure the axial pressure drop and differences in pressure between the two channels at several locations. A pair of pressure taps were located 1/2 in. downstream from the end of the heated section within the electrical connections. Pairs of taps were also located 6 and 12 in. upstream from the outlet end of the heated section to measure subchannel pressure differences. Actual system pressure was measured with Heise gauges and differential pressures with inclined* and vertical* Mercury manometers. Each pressure tap line leading from the test section was horizontal before entering a small accumulator. These accumulators, normally near ambient temperature, condensed any vapor drawn through the pressure tap and prevented hot water from entering vertical legs of the tap lines.

The test section was fitted with Inconel sheathed Iron-Constanton thermocouples welded to selected positions on the outer surface of the heated section. These temperatures were observed during test section power increases to detect the possible occurrence of boiling burnout.

TEST PROCEDURE

Isothermal runs (zero test section power) were initially performed to calibrate thermocouples and to determine heat losses from various parts of the system. They were conducted by setting the desired test section pressure, flow and inlet temperature, and recording the desired data. Flows through the test section inlet and outlet piping were adjusted to give

---

* *Inclined manometers read to ±0.01 in. Mercury; vertical manometer read to ±0.01 psi.*

approximately zero cross channel pressure difference at the exit of the test section. During operation of the electric preheater, erroneous flow signals were produced by the flow meters in the separated inlet streams; therefore, the flow split in the inlet piping was preset prior attaining system temperatures greater than about 200 °F. This flow split was assumed to exist for higher inlet temperatures and was checked after each shutdown of the preheater.

For a series of power runs at a given inlet temperature, pressure, and flow rate, the initial isothermal condition was established and all data was recorded. The test section power was then gradually raised to a selected power level. If boiling had begun, or was occurring, the flow split at the test section outlet was adjusted to give zero pressure differential between the two channels at the end of the heated section. Once the system stabilized and no further adjustment was necessary, the data was recorded. The same procedure was repeated for each selected power level at that flow and inlet temperature condition.

Experiments were conducted using two simulated rod spacings. The first was a spacing of 0.084 in. and corresponded to the nominal dimensions of the inlet and outlet test section fittings. The second simulated rod spacing of 0.020 in. was achieved by adjusting the shims in the support block assembly. The shim adjustment was made in such a way that the ratio of the hydraulic diameters was nearly preserved, thus, nearly preserving the flow split. This permitted use of the same test section end fitting. It also helped minimize any flow redistribution that could occur at the 2 in. transition from 0.020 in. spacing to the 0.080 in. spacing of the end fittings at each end of the heated section.

METHOD OF DATA REDUCTION

Raw data, recorded on data sheets and punched paper tape, was processed by transferring this data to punched cards that

provided input to a digital computer program. This program was run in two stages to accommodate isothermal runs and then the power runs. This gave much more rapid and consistent data reduction than was possible to do by hand calculation.

During the reduction of isothermal run data, temperatures were converted from their millivolt readings to actual temperature using a standard calibration for Iron-Constanton thermocouples; also the RTD readings were converted to temperature using their appropriate calibration curve. Flows were converted from their milliampere valves to mass flow rate using the flow meter calibration curves and density obtained from the water temperatures. Pressure drop readings were converted to psi and corrected for the elevation difference between pressure taps.

The primary purpose of the isothermal run calculations was to determine corrections to thermocouples and determine heat loss. The thermocouples corrections were determined by plotting the difference between the thermocouple temperature and a reference RTD temperature versus the reciprocal of the mass flow rate at some system temperature. The intersection of a line drawn through these points with the temperature axis gave the thermocouple correction. The corrections at several system temperatures were used to define a correction curve for the thermocouple temperatures. Generally, these corrections were less than about 2 °F.

The isothermal run data also provided heat loss information from various parts of the system. Only losses from the inlet and outlet piping of the test section were significant; no significant losses occured from the heat exchangers.

The thermocouple corrections and heat losses were incorporated into the data reduction program for the power runs. The program was revised to accommodate these changes and was set up to compute test section power, heat flux, and average exit

enthalpy. The program also computed the test section subchannel exit enthalpy from a heat balance on the heat exchangers. Error calculations were also performed as outlined in Appendix A.

RESULTS

Two sets of experiments were conducted at a system pressure of 900 psia. In the first set of experiments with a simulated rod spacing of 0.084 in., data were taken at selected values of heat flux for inlet temperatures of 330 °F and 510 °F and average mass velocities of 1.0, 2.0, and 3.0 x 10^6 lb/hr-ft^2. Maximum heat flux for a set of flow and temperature conditions was about 2/3 of the burnout heat flux predicted from previous 0.080 in. spaced 19-rod bundle burnout data. In the second set of experiments, a simulated rod spacing of 0.020 in. was used. This was achieved by adjusting shims in the test section support blocks so that the simulated rods were deflected inward. The resulting flow channel had a simulated rod spacing of 0.020 in. over most of its length with the exception of a 2 in. transition back to the original 0.080 in. spacing in the electrical connectors. Channel flow areas for the 0.020 in. spacing were chosen to maintain the area ratio of the two channels equal to the ratio of the 0.084 in. spacing in order to minimize any flow diversion effects at the spacing transition at either end (Figure 4). Nearly the same set of experimental conditions was used for this set of experiments as was used for the 0.080 in. spaced section. Only the case of the 510 °F inlet and mass velocity of 1.0 x 10^6 lb/hr-ft^2 was not run for the 0.020 in. spacing.

SUBCHANNEL EXIT ENTHALPY

Plots of the subchannel enthalpy rise, through the test section and subchannel flow rate versus heat flux, are shown in Figures 5 through 15. Each figure represents the exit conditions for a simulated rod spacing, flow rate, and inlet temperature. By comparing the plots with the same spacing and flow, but at the two inlet enthalpies of 300 and 500 Btu/lb, the differences in the amount of mixing between nonboiling and boiling conditions

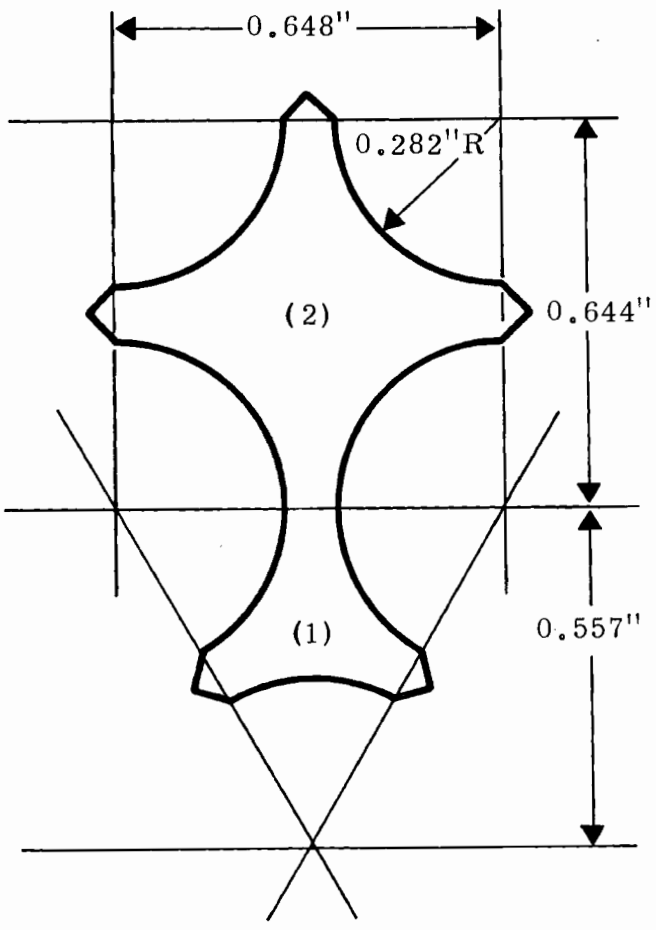

Channel Dimensions, 0.084" Gap

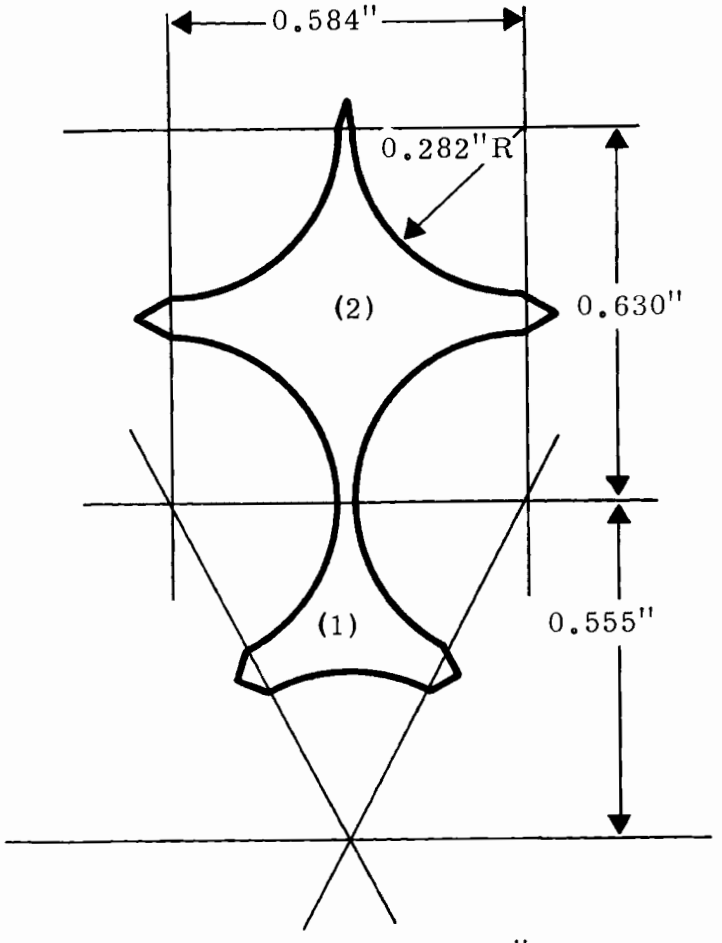

Channel Dimensions, 0.020" Gap

FIGURE 4. Subchannel Cross Section Dimensions for 0.084 and 0.020 in Simulated Spacing

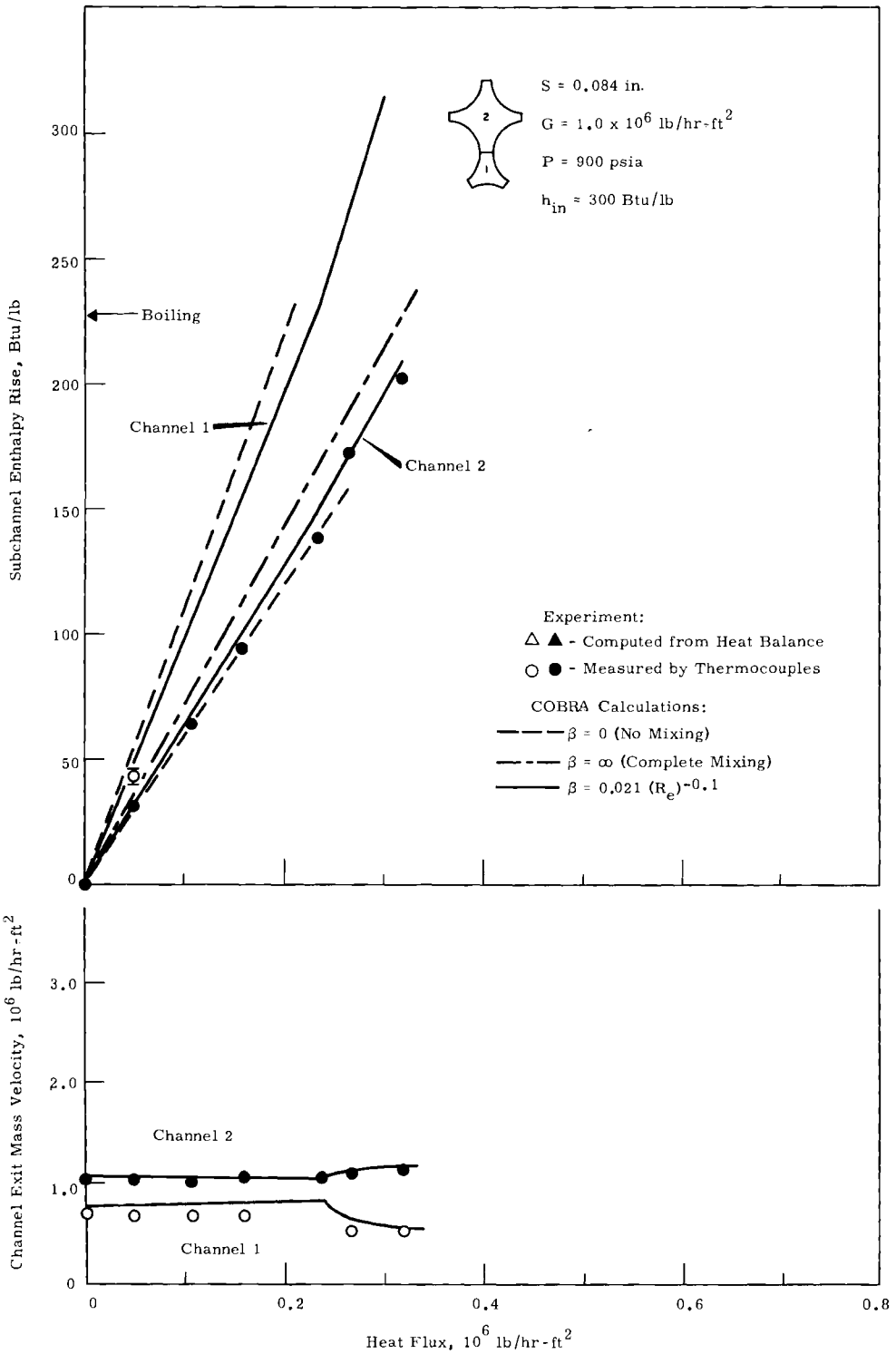

FIGURE 5. Subchannel Enthalpy Rise and Exit Flow Rate at G = 1.0 x 10^6 lb/hr-ft^2 and 0.084 in. Spacing

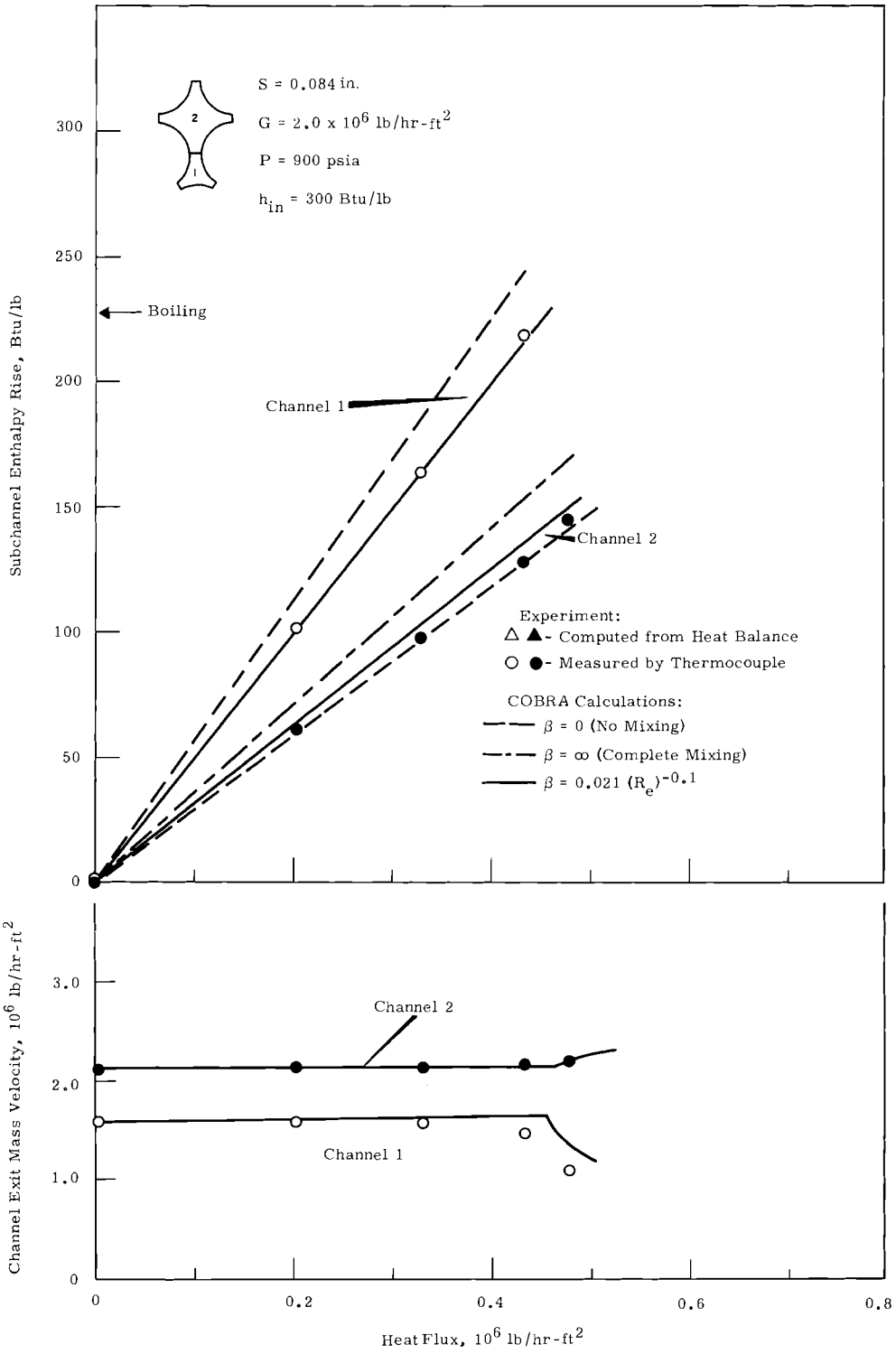

FIGURE 6. Subchannel Enthalpy Rise and Exit Flow Rate at G = 2.0 x 10^6 lb/hr-ft^2 and 0.084 in. Spacing

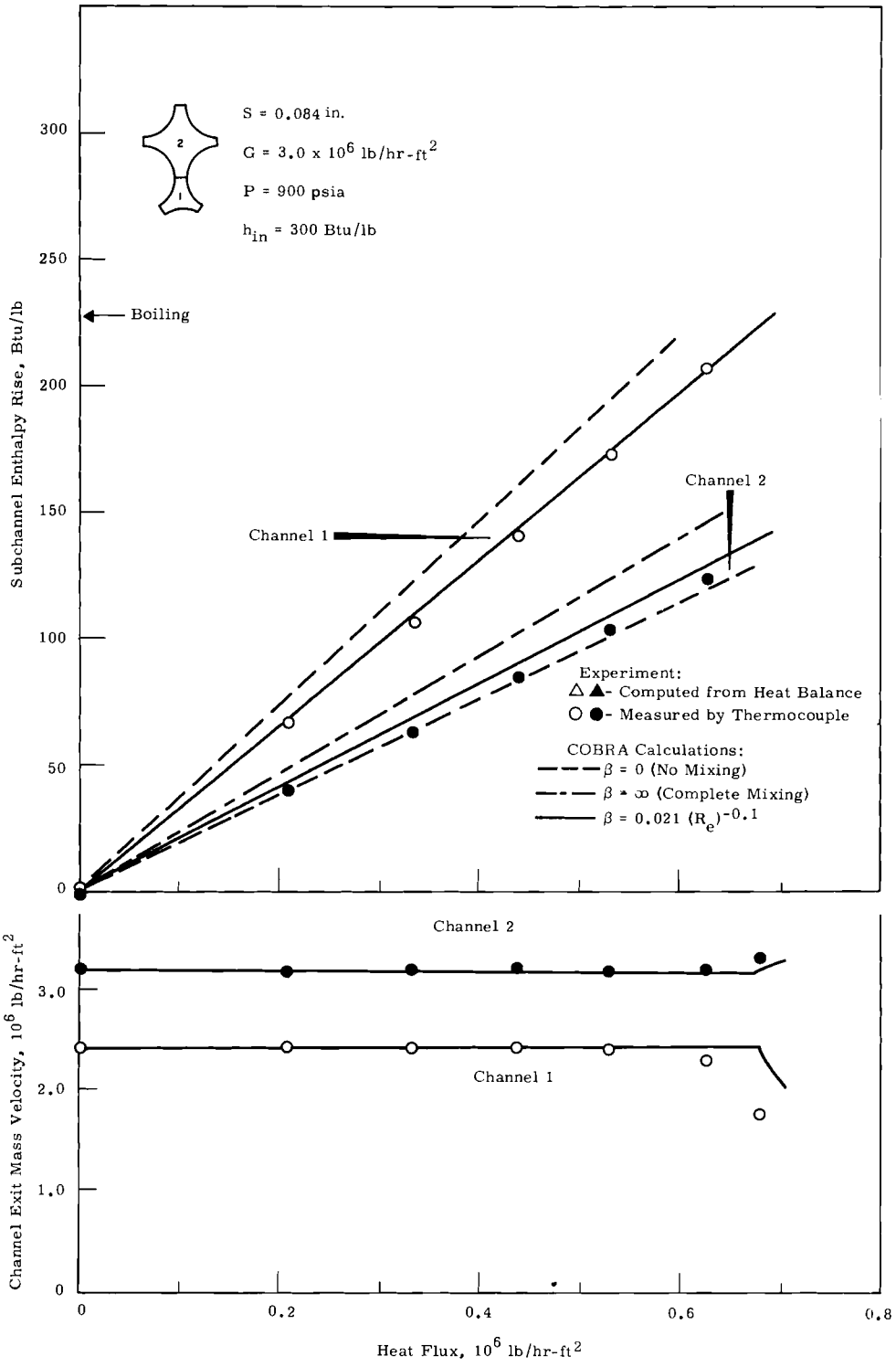

FIGURE 7. Subchannel Enthalpy Rise and Exit Flow Rate at G = 3.0 x 10^6 lb/hr-ft^2 and 0.084 in. Spacing

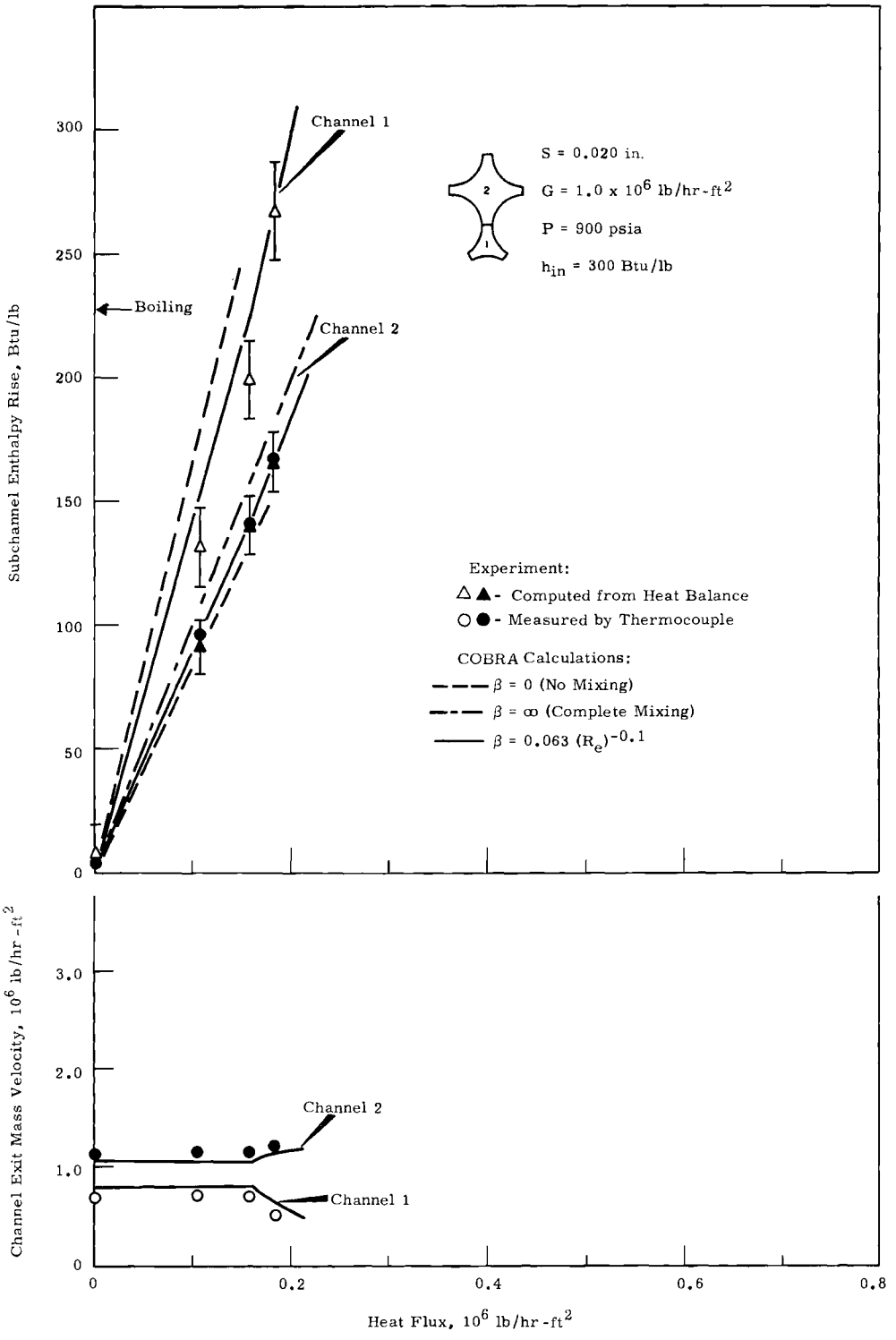

FIGURE 8. Subchannel Enthalpy Rise and Exit Flow Rate at G = 1.0 x 10^6 lb/hr-ft^2 and 0.020 in. Spacing

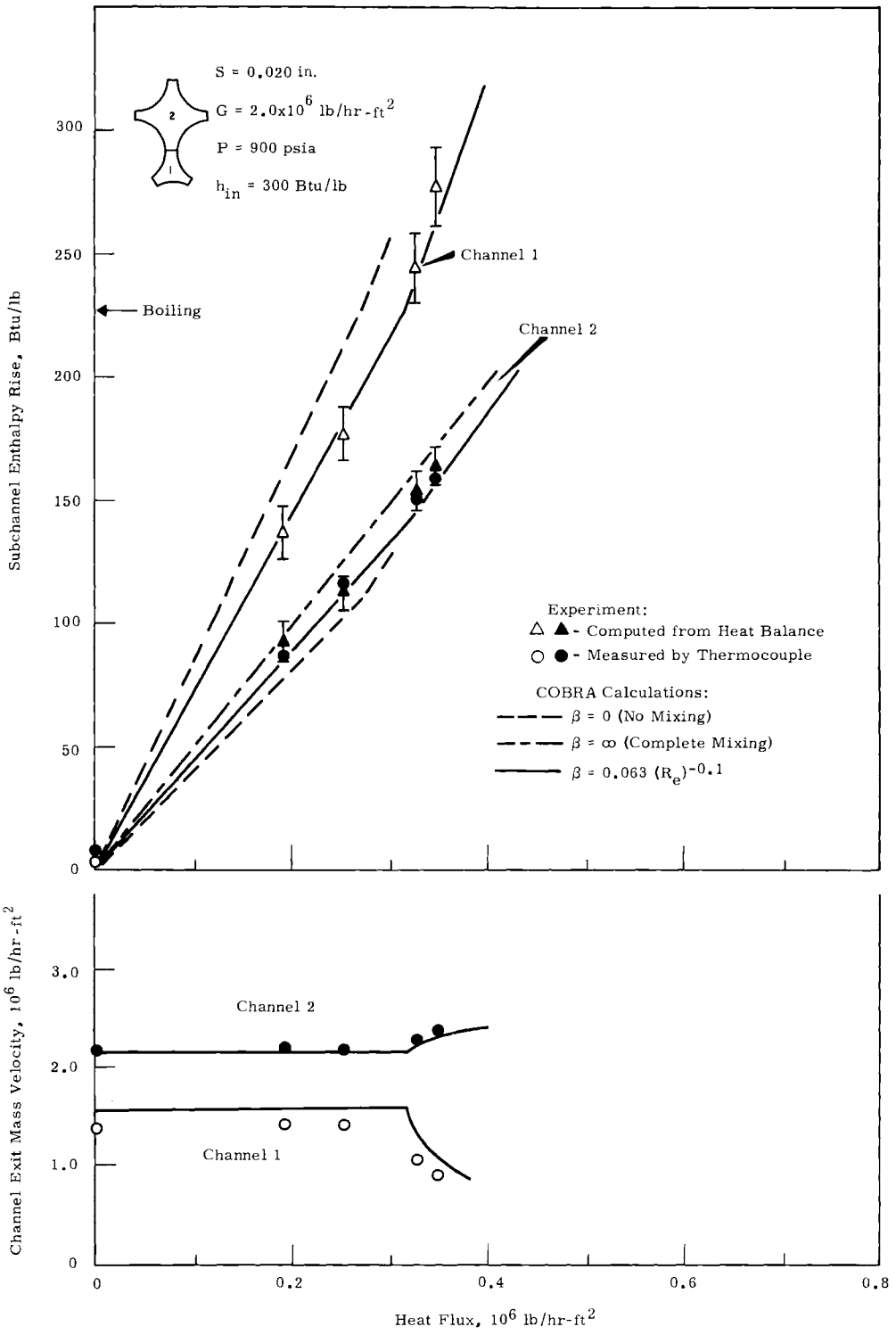

FIGURE 9. Subchannel Enthalpy Rise and Exit Flow Rate at G = 2.0 x 10^6 lb/hr-ft^2 and 0.020 in. Spacing

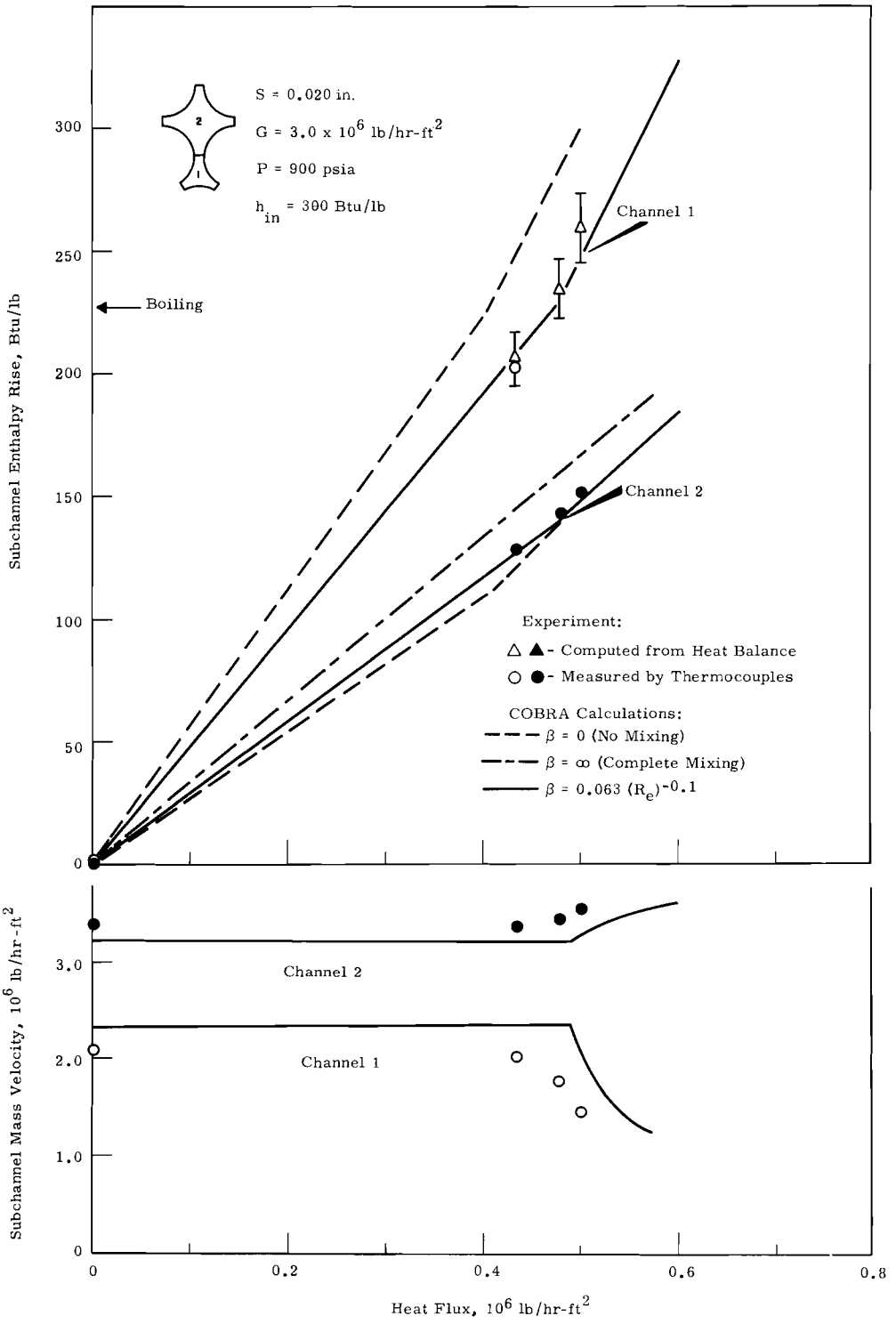

FIGURE 10. *Subchannel Enthalpy Rise and Exit Flow Rate at G = 3.0 x 10^6 lb/hr-ft^2 and 0.020 in. Spacing*

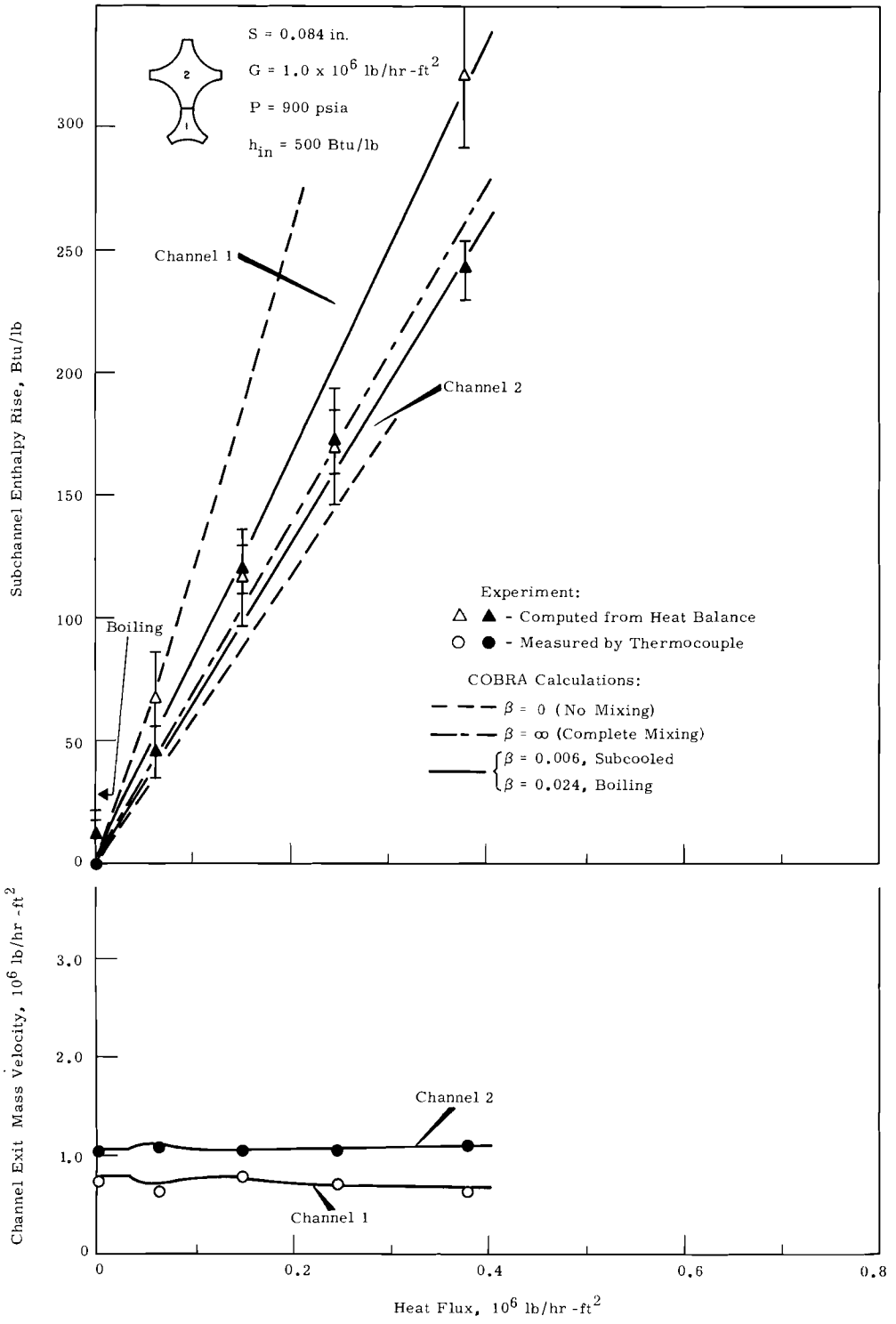

FIGURE 11. Subchannel Enthalpy Rise and Exit Flow Rate G = 1.0 x 10^6 lb/hr-ft^2 and 0.084 in. Spacing

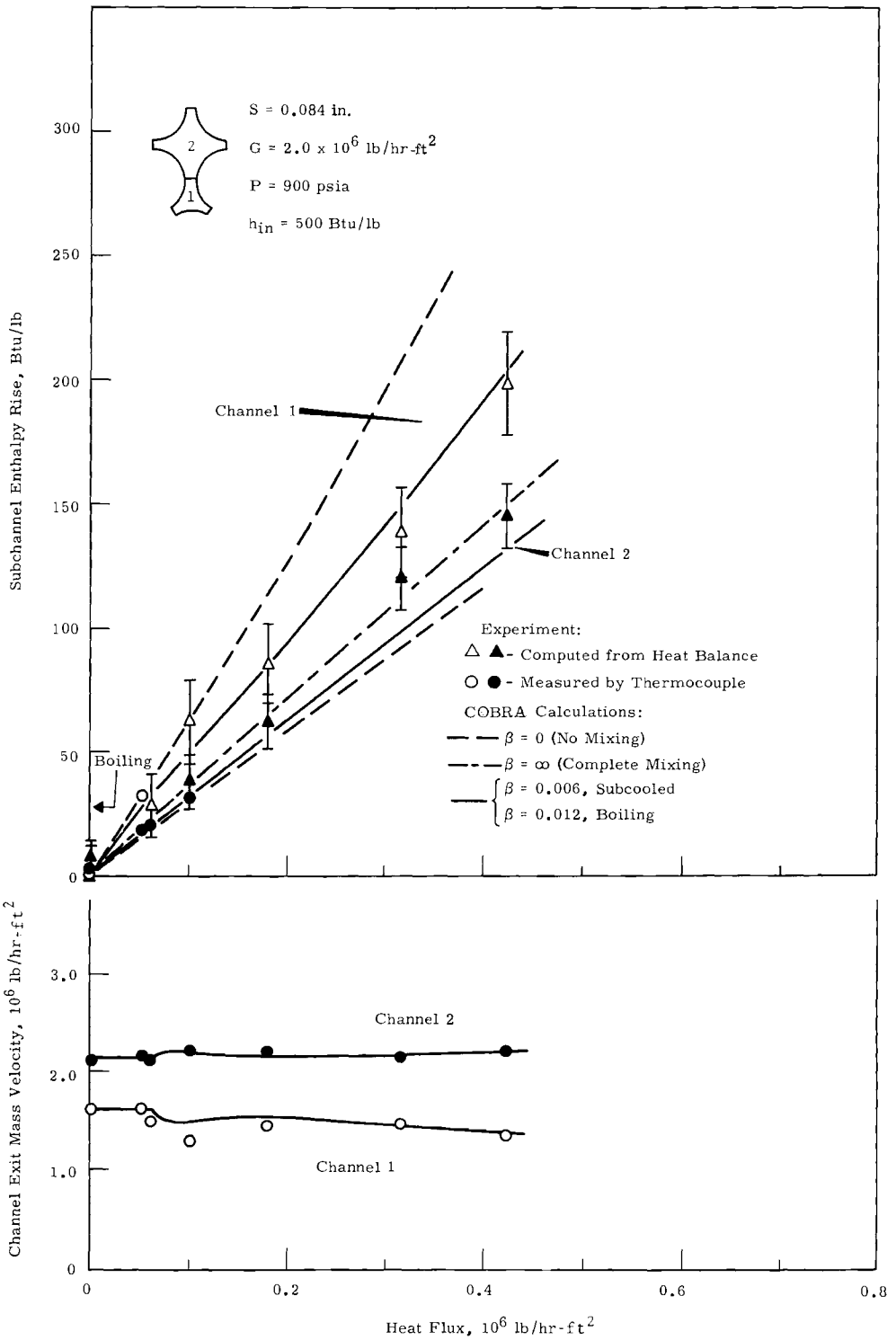

FIGURE 12. Subchannel Enthalpy Rise and Exit Flow Rate at G = 2.0 x 10^6 lb/hr-ft^2 and 0.084 in. Spacing

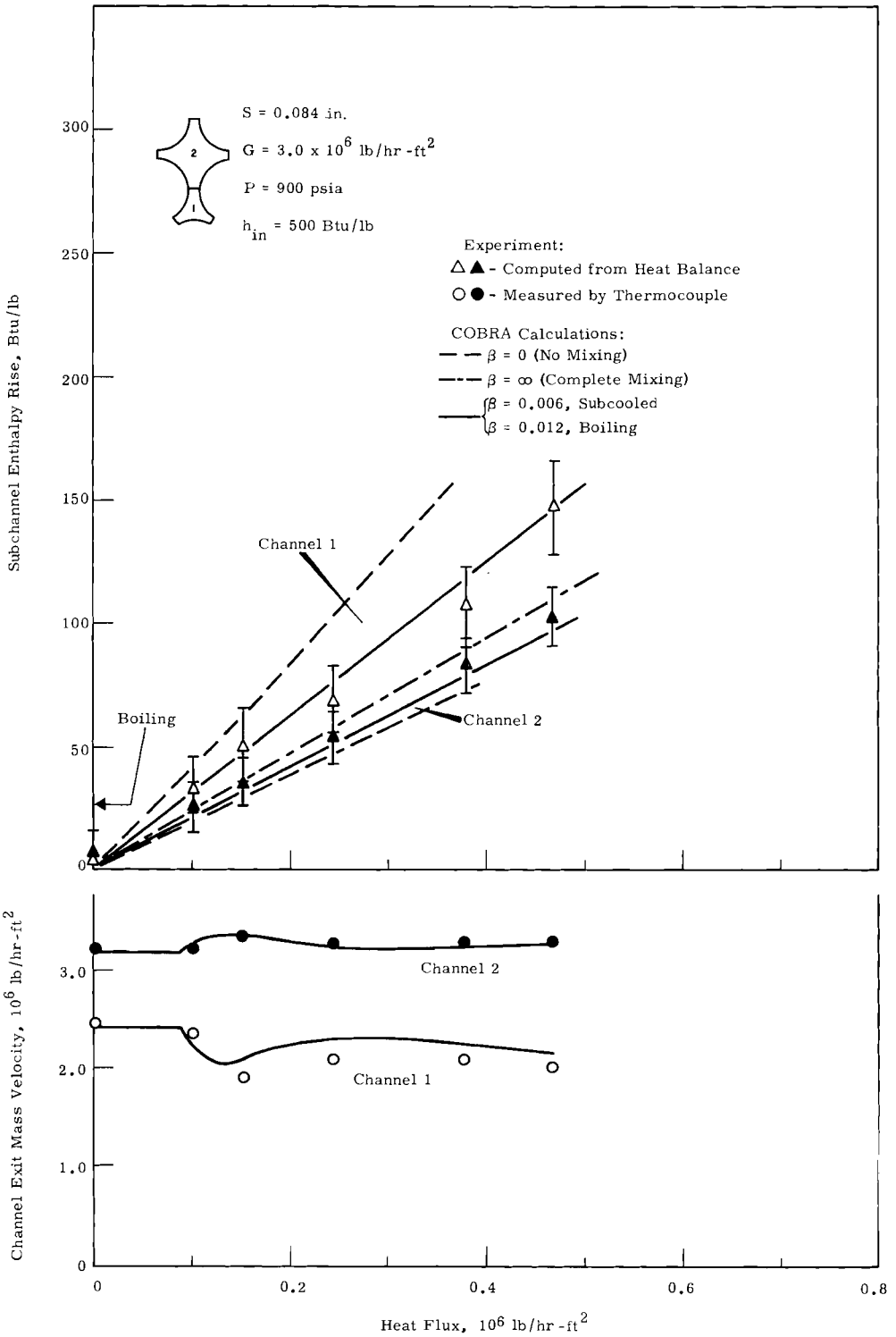

FIGURE 13. Subchannel Enthalpy Rise and Exit Flow Rate at G = 3.0 x 10^6 lb/hr-ft^2 and 0.084 in. Spacing

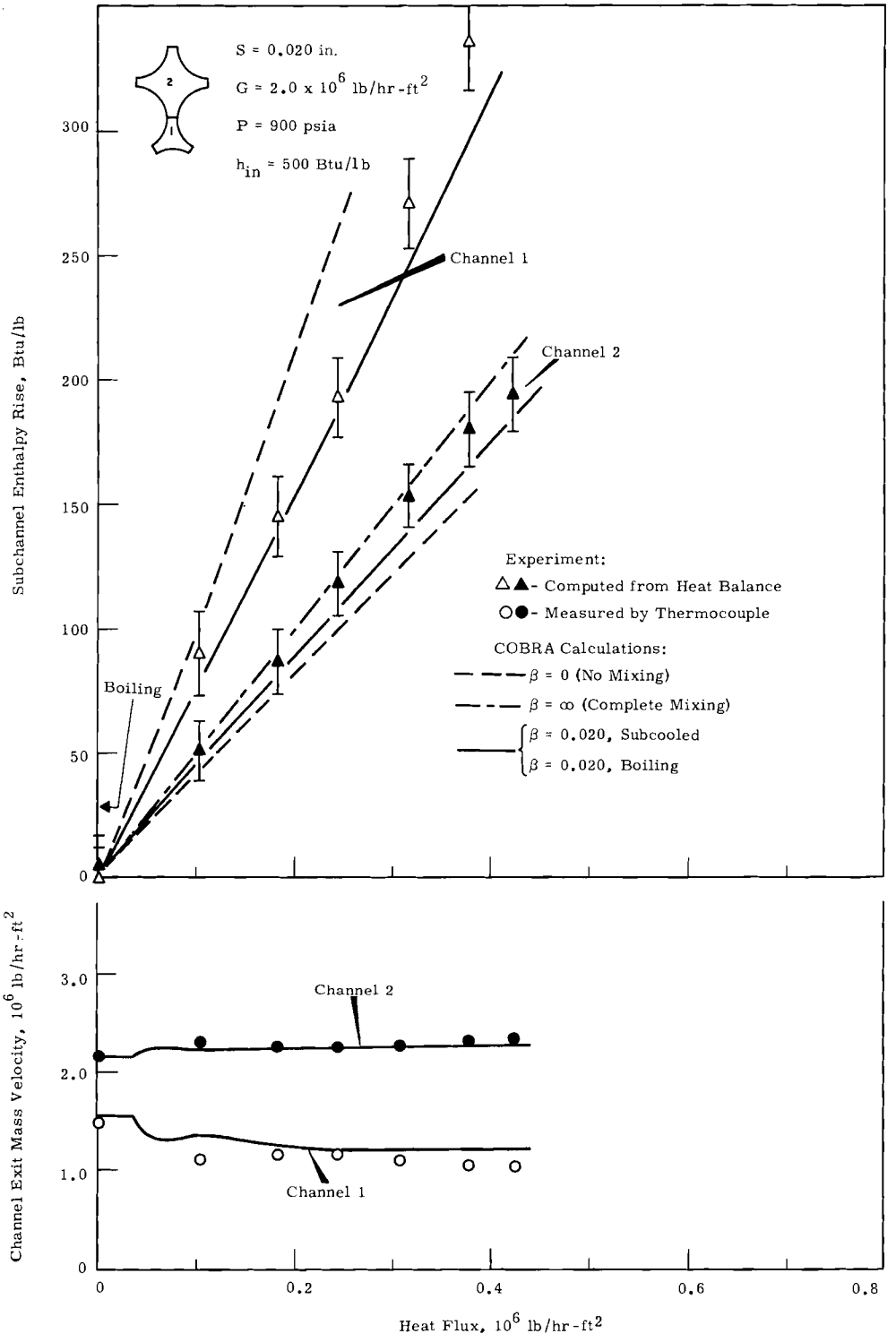

FIGURE 14. Subchannel Enthalpy Rise and Exit Flow Rate at G = 2.0 x 10^6 lb/hr-ft^2 and 0.020 in. Spacing

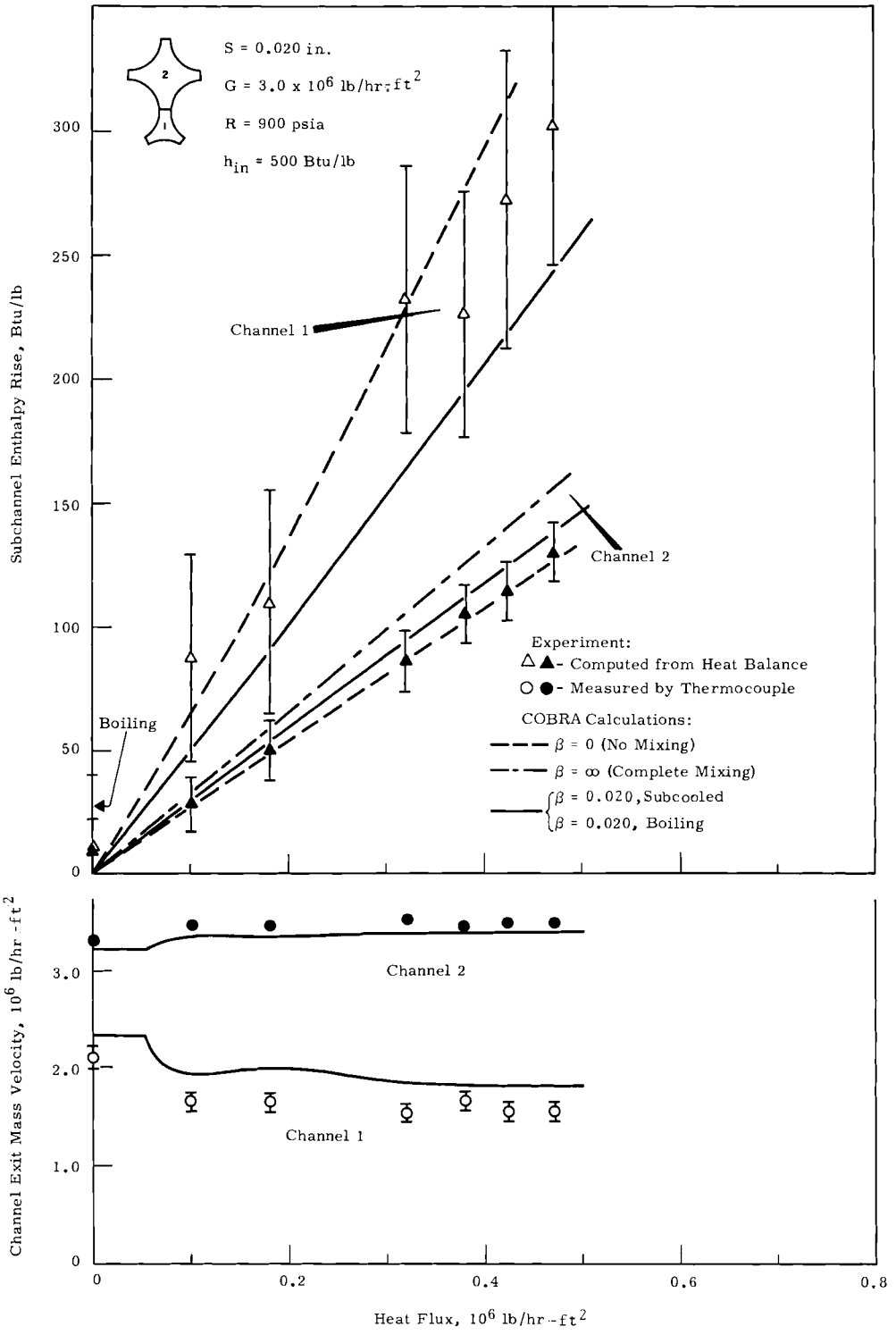

FIGURE 15. Subchannel Enthalpy Rise and Exit Flow Rate at G = 3.0 x 10^6 lb/hr-ft^2 and 0.020 in. Spacing

can be seen. It is apparent that improved mixing during boiling occurs for the 0.084 in. spacing, but little, if any, improvement occurs during boiling with the 0.020 in. spacing. A more detailed discussion of the amounts of mixing will be presented later in the report.

The error bars shown on the data points are representative of possible errors caused by the method of data reduction as detailed in Appendix A. While they are not true statistical errors, they reveal the relative validity of the data. Comparison between the enthalpy rise obtained with the thermocouples and the heat balance show that the heat balance errors are generally not as large as indicated by the error bars.

SUBCHANNEL EXIT FLOW

Mass velocity for the subchannels are plotted in Figures 5 through 15 as a function of heat flux. For the low inlet temperature cases, the change in flow prior to bulk boiling indicates the presence of subcooled void formation. Once bulk boiling begins, significant flow diversion occurs; and, as could be expected, the smaller channel flow decreases significantly. For the higher inlet enthalpy, the flow redistribution is not as severe; and once boiling is established in both channels only moderate flow redistribution occurs.

Axial Pressure Drop

Pressure drop of the heated section is plotted as a function of heat flux in Figures 16 and 17 for the 500 Btu/lb inlet enthalpy and the two rod spacing. This is the actual pressure difference between the ends of the heated section and is composed of the frictional, acceleration, and elevation components of pressure drop. As could be expected, the pressure drop increases with heat flux during boiling.

Transverse Pressure Drop

The pressure differences between subchannels were found to be small. Because some bias existed on the data, probably caused

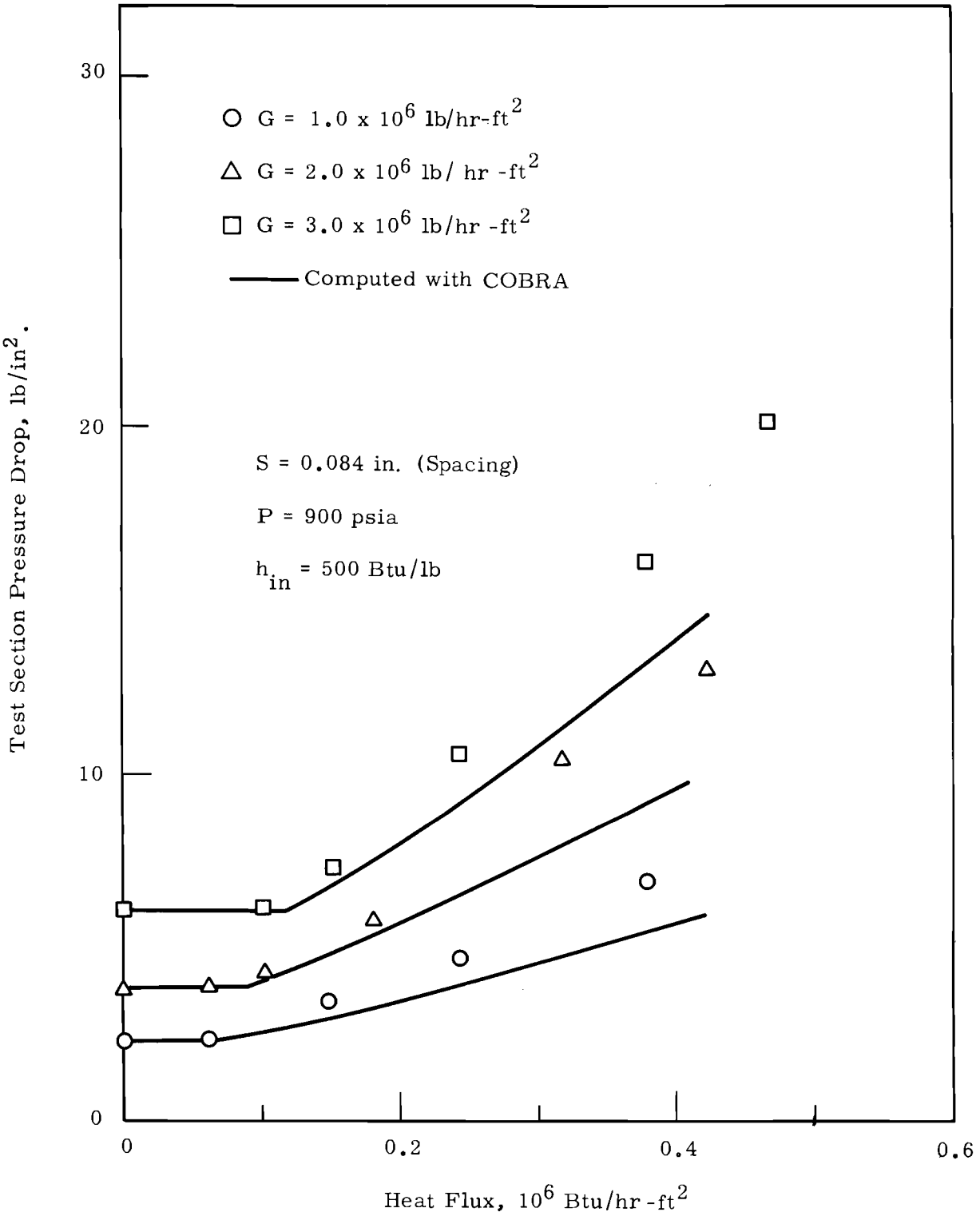

FIGURE 16. Test Section Pressure Drop During Boiling with 0.084 in. Spacing

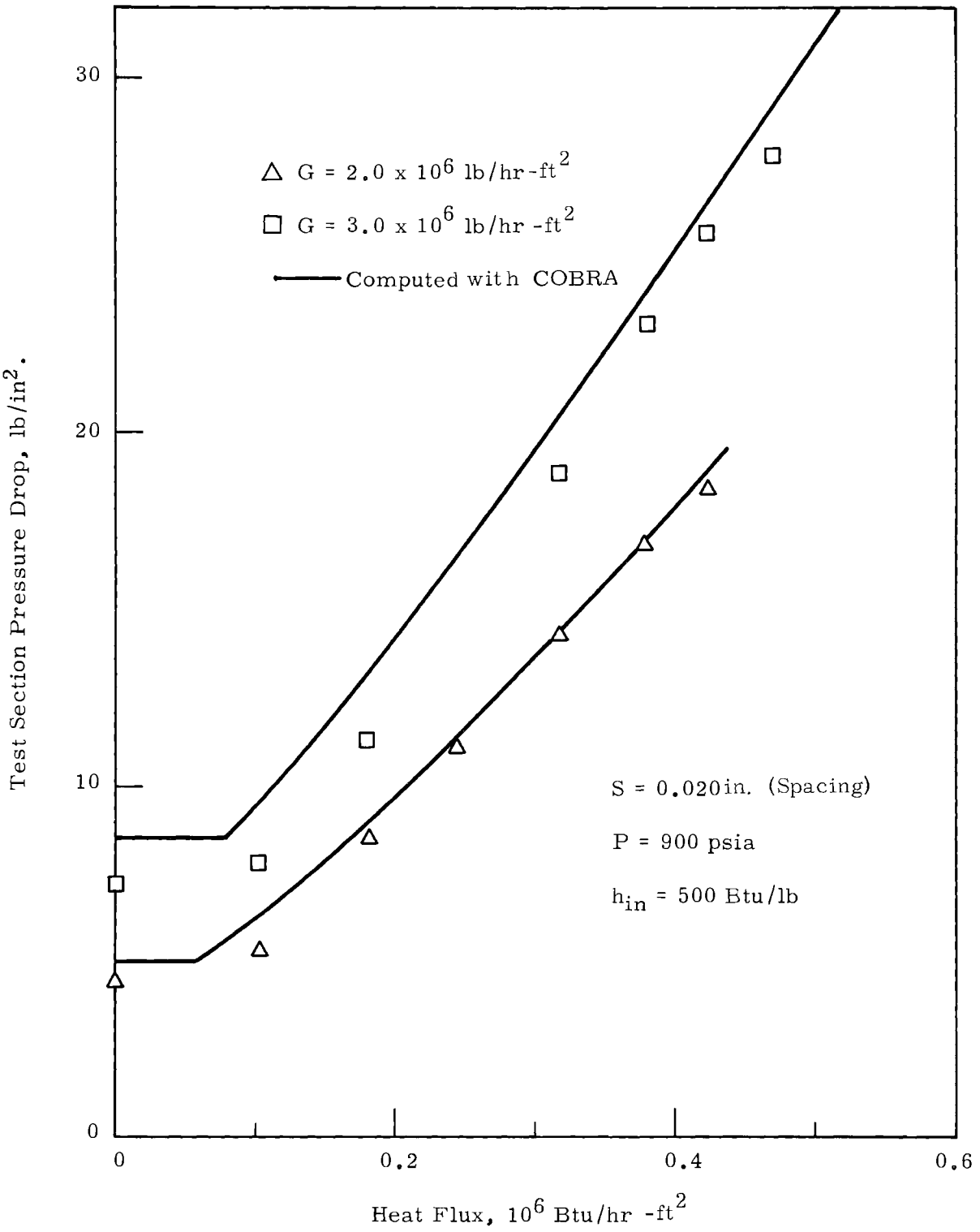

FIGURE 17. Test Section Pressure Drop During Boiling with 0.020 in. Spacing

by imperfect pressure taps, exact data can not be reported; however, by comparing the changes during boiling an estimate of the transverse pressure drop can be made. Comparison of the transverse pressure drop data in Table I shows small changes for the 0.084 in. spacing during boiling. For the 0.020 in. spacing, slightly larger pressure differences are seen during boiling; but again, they are not very large. For both spacings, the transverse pressure drops are largest for the highest test section flow rates.

OBSERVATION DURING EXPERIMENTS

Heat Exchanger Temperature Fluctuations

During initial runs of the experiment, temperature fluctuations were noted in the cooling water outlet from the subchannel heat exchangers. We thought that film boiling was occurring on the cooling side, and was causing fluctuations in the heat transfer coefficient; therefore, a pressurizing pump was used to pressurize the cooling side thus reducing the probability of film boiling.

Pressurizing the cooling side of the heat exchanger helped reduce the exit temperature fluctuations but, some fluctuations still remained. The remaining fluctuations were eliminated by changing the operation of the heat exchangers from counterflow to parallel flow. This allowed the outlet streams from the heat exchangers to exit with much less temperature difference.

Subchannels Flow Oscillations

During the experiments with the lower inlet temperature, significant flow oscillations were observed as indicated in Table I.

TABLE I. Observed Flow Oscillations

Run	Mass Velocity (10^6 lb/hr-ft^2)	Heat Flux (10^6 Btu/hr-ft^2)	Percent Flow Oscillation	Period of Oscillation, sec
31	3.00	0.679	±8	8
36	1.99	0.476	±5	7
45	0.97	0.319	±2	4

These were noticed at a mass velocity of 3 x 10^6 lb/hr-ft^2 with a simulated rod spacing of 0.084 in. and at a heat flux to cause bulk boiling in the small subchannel at the exit of the test section. At higher heat fluxes, progressively larger flow oscillations were observed; and, because of the severity of the flow oscillations, heat flux was not increased enough to cause boiling in the larger subchannel. During runs at a mass velocity of 2 and 1 x 10^6 lb/hr-ft^2, similar behavior was noted; but with reduced period and magnitude of the oscillations. Since the oscillations at a mass velocity of 1 x 10^6 lb/hr-ft^2 were not very severe, heat flux was increased enough to cause boiling in the larger subchannel; however, just as boiling started, a very severe flow of oscillation occurred and caused a rapid rise in all test section thermocouples. Damage to the test section was prevented by an immediate reduction in power; but, the thermal shock during re-establishment of flow caused some leaks to develop in the electrical connection braze joints.

During runs with the smaller spacing of 0.020 in. and the lower inlet temperature, very similar behavior was observed; however, heat flux, was only increased enough to establish boiling and the existence of the flow oscillations. For the runs with the higher inlet temperature and both spacings, only small flow oscillations were encountered. These small flow oscillations were generally less than 2% of the total flow with rather erratic fluctuations.

The cause of these flow oscillations is not entirely clear. The piping to each flow channel before entering the test section provided considerable pressure drop as compared to the heated section and downstream piping. This would tend to rule out parallel channel flow instability of the two channels when the inlet piping resistance is considered.

In the heated section it is possible that instabilities between the two interconnected parallel channels could occur, though a detailed explanation of this is not possible at this time. It is conceivable that the oscillation could be produced by the cooler stream alternately quenching the boiling stream. If a small amount of cool water was diverted across the gap to the smaller boiling subchannel, the pressure would reduce in the boiling stream and cause additional cool water to be diverted and cause additional quenching. The reduction of the steam void would cause an increase in flow to the test section. Once the void collapse stops from the quench, boiling in the test starts new void formation that causes a reduction in flow to the test section. The cycle then repeats, leading to sustained oscillations.

Flow Split Sensitivity

The flow split from the heated section was adjusted to give equal static pressure between the two channels at the end of the test section. To determine the sensitivity of this adjustment, a series of cold hydraulic tests were run with the 0.084 in. spacing to determine the subchannel pressure difference as a function of the exit flow split. The results of these tests can be seen in Figure 18; and, as would be expected, the greatest sensitivity is obtained at the higher flow rates. An interesting observation during these runs was that for all data points, and even with the small subchannel blocked completely at the exit of the test section, no change in the pressure difference between subchannels was observed just 6 in. upstream from the outlet end.

This means that either the flow diversion occurred over a very local area or the crossflow resistance is very small, or both.

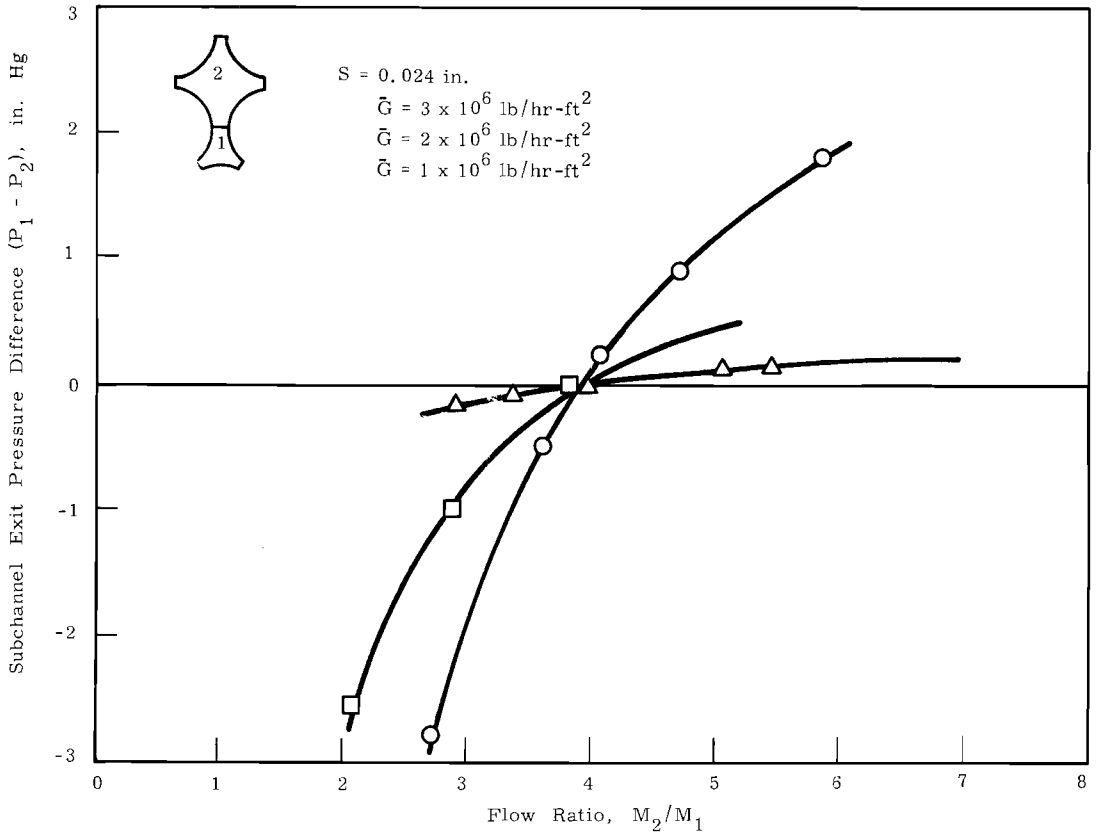

FIGURE 18. Cold Water Hydraulic Test Results to Determine Flow Split Sensitivity

DISCUSSION

In the first part of this study[1] an analytical model was developed to describe the local pressure, flow and enthalpy in rod bundle subchannels as influenced by two types of thermal mixing that occur between adjacent subchannels. The first type of mixing is caused by the net convective transport (diversion crossflow) of energy from one subchannel to another. This type of mixing would result from flow redistribution* when pressures try to equalize as boiling coolant flows through the bundle.

---

* *Diversion of flow from one subchannel to another could occur from other effects such as channel blockage, wire wraps, etc.*

Mixing of this type can be computed with reasonable accuracy from the momentum and energy equations.

The second, and remaining, mixing effect is attributed to the turbulent exchange that occurs between adjacent subchannels. It is assummed to be superimposed upon the diversion component of mixing. Formulation of this turbulent thermal mixing for boiling is an extension of the single-phase treatment of turbulent flow, and is of the form $\omega' \Delta h/m$ where ω' is a fluctuating mass flow rate per unit length; Δh is the enthalpy difference between the adjacent subchannels; and m is the flow rate of the subchannel under consideration. The fluctuating crossflow is further defined as

$$\omega' = s\beta\bar{G} \qquad (1)$$

where β is a dimensionless mixing parameter; s is the gap spacing; and $\bar{G}$ is average mass velocity of the two adjacent subchannels. This formulation of ω' assumes that the random travel of the two-phase mixture between adjacent channels causes no net change in flow when averaged over a short period of time.

The value of the mixing parameter β is the most significant of several uncertain or unknown parameters of the mathematical model. The value of β must be found experimentally since no methods are presently available to compute it. From the results of the experiments presented in this report, the values of β can be determined for both single-and two-phase flow. The approach used is to first determine the amount of turbulent mixing that gives agreement between the computed and experimental subchannel exit enthalpies for subcooled conditions; and next to determine the amount of turbulent mixing that gives agreement between the computed and experimental subchannel exit enthalpies for boiling conditions, assuming that single-phase mixing applies up to the time bulk boiling occurs, and that the superposition of the two types of crossflow is valid.

SINGLE-PHASE MIXING

Mixing during single-phase flow is quite uniform for fully developed turbulent flow; therefore, constant values of β were used in COBRA to compute subchannel exit enthalpy for the nominal conditions of the experiment. By comparing the experimental and computed values of exit enthalpy, values of β = 0.006 and 0.020 were selected for the two rod spacings of 0.084 and 0.020 in., respectively. Calculations using these values of β gave quite good agreement with the data; but they did not agree with some of the trends exibited by the experimental data such as poorer mixing with increased temperature and increased flow rate. Both of these rather small effects can be explained using Reichardt's[3,4] method for correlating eddy diffusivity.

Since the eddy diffusivity for heat has the same mathematical form as the eddy diffusivity for momentum, we can write

$$\varepsilon_q \propto \frac{D\sqrt{\tau_\omega g_c}}{\rho} \quad . \tag{2}$$

By using the definition of wall shear stress for turbulent flow,

$$\tau_\omega = \frac{f}{8} \frac{\rho U^2}{g_c}, \tag{3}$$

the eddy diffusivity can be written as

$$\varepsilon_q \propto uD\sqrt{\frac{f}{8}} \quad . \tag{4}$$

The friction factor is often correlated as

$$f = a\,(R_e)^b; \tag{5}$$

therefore,

$$\frac{\varepsilon_q}{uD} = K\,(R_e)^{b/2} \quad . \tag{6}$$

From the development of COBRA, the turbulent heat transport per unit length can be approximated by

$$q_t' = \varepsilon_q\, s\, \rho\, C_p \frac{\partial t}{\partial y} \tag{7}$$

or writing an approximation for the partial derivative

$$q_t' = \varepsilon_q \, s \, \rho \, \frac{\Delta h}{\Delta y} \quad . \tag{8}$$

The right side of Equation (8) is equivalent to the term $w'\Delta h$ in the development of COBRA; therefore,

$$w' = \frac{\varepsilon_q \, s \, \rho}{\Delta y} \quad . \tag{9}$$

The quantity w' is also written as

$$w' = \beta s \rho u \quad . \tag{10}$$

From Equations (9) and (10), the mixing parameter β can be written as

$$\beta = \frac{\varepsilon_q}{u \Delta y} \tag{11}$$

or using Equation (6)

$$\beta = \frac{KD}{\Delta y} (R_e)^{b/2} \quad . \tag{12}$$

Proper choice of the constants in Equation (12) is rather difficult. For a given geometry, the product $KD/\Delta y$ should be a constant. To determine the value of the constants ($KD/\Delta y$ and $b/2$), several values were chosen and calculations were performed with COBRA to determine the subchannel exit enthalpy. Comparison of the calculations and experimental data showed that

$$\beta = 0.021 \, (R_e)^{-0.1} \qquad (s = 0.084 \text{ in.}) \tag{13}$$

and

$$\beta = 0.063 \, (R_e)^{-0.1} \qquad (s = 0.020 \text{ in.}) \tag{14}$$

would satisfy the data (Figures 5 through 10). It should be realized that the exponent (-0.1) in Equations (13) and (14) is not a strong parameter. A considerable error in this value, but consistent with the value of $KD/\Delta y$, would not cause a significant error in β for changes in Reynolds Number.

The constant K in Equation (12) should be about the same for similarly shaped flow channels. If this is so, then the relative

values of Δy for the two simulated rod spacings can be determined from the constant values $(KD/\Delta y)$ in Equations (13) and (14). A comparison of the values is shown in Table II.

TABLE II. Correlation Constants

s	$(KD/\Delta y)$	$D^{(a)}$	$\Delta y^{(b)}$
0.084	0.021	0.287	0.0847
0.020	0.063	0.201	0.0198

(a) $D = 4\ (A_1 + A_2)/(P_1 + P_2)$
(b) *Assuming* $K = 0.0062$

It is interesting that Δy is very close to the gap spacing (s) for the chosen value of K = 0.0062. This is rather surprising, because Δy could easily be assumed to be equal to the relative distance between the two channels.[5,6] This would follow from the difference approximations of Equation (9). The reason Δy is proportional to rod spacing for these experiments is not known for sure; but, since the scale of turbulence is governed by the channel dimensions, the gap could be controlling the scale of Δy. If the observation that Δy is proportional to s is used in Equations (13) and (14), we can write a correlation for β as

$$\beta = 0.0062\ \frac{D}{s}\ (R_e)^{-0.1} \qquad (15)$$

There are obvious limitations to Equation (15) and the reasoning that says Δy is proportional to s. For zero spacing no mixing can occur, and for very large spacing Δy is limited by the dimensions of the subchannels. Additional work will have to be done to determine the influence of these extreme conditions. For the present time it seems reasonable that Equation (15) would be valid for rod bundles with geometric dimensions or pitch-to-diameter ratios that are comparable to these experiments.

The significance of Equation (15) is that it should give the lower limit of mixing in a multirod bundle. Actual rod bundles will have rod spacers such as wire wraps that can force flow diversion and induce higher levels of turbulence.

A fairly good test of Equation (15) can be made with the experimental results of two separate experiments performed by Westinghouse.[7,8] Both of these experiments were performed to determine turbulent mixing by using tracers and square arrays of 64 and 144 rods. Rod spacings of 0.043 and 0.064 in. were considered with the 64 rod array, and 0.082 in. with the 144 rod array. All these experiments gave a mixing parameter value of about $\varepsilon/uD = 0.003$ with only little variation with Reynolds Number. A direct comparison of this mixing parameter to Equation (16) can be made because from the development of COBRA and the analytical study of mixing by Grimble and Bell[9]

$$\frac{\beta_s}{D} = \frac{\varepsilon}{uD} \quad ; \tag{16}$$

which also follows from Equation (12) for $\Delta y = s$.

Equation (15) gives, for $R_e = 20{,}000$, $\beta_s/D = 0.0023$ which is about 30% lower than the value obtained at Westinghouse for a similar Reynolds Number. There are several reasons why their values could be higher. Bell and Le Tourneau[7] reported that, "Dye concentration observed in channels symmetrically located with respect to the center channel injection channel showed variations up to 300%. It is believed that these anomalies are the result of imperfect test models. These models, which had been previously used in pressure drop studies, had become distorted, somewhat, in the process of assembly and disassembly. Also the 30-in. rods tended to sag at the center, causing the rod spacing to be nonuniform." It seems quite reasonable that the level of mixing caused by flow diversions within this bundle could cause higher levels of mixing than is found in the present experiments. In the other experiments[8] rod spacing was

maintained with segments of thin wall tubing (ferrules) placed at intervals within the flow channel. These spacers would maintain the rod alignment, but could have introduced additional turbulence, thus causing higher rates of mixing than if they were not present. When these factors are considered it seems that there is reasonably good agreement between the present experiments and the Westinghouse experiments.

Mixing experiments were performed with a 19-rod hexagonal bundle for the CVTR[10] using a Lithium ion tracer. For the case of no wire wraps on the rods, the results gave about three times the level of mixing found in the present experiments. Two possible reasons for this are turbulence introduced by the inlet end fitting and flow redistribution within the bundle at the inlet. The flow redistribution could be rather significant because the fully developed flow velocities in the outer flow channels were about 2.6 times those in the central part of the bundle. Any flow redistribution that occurs at the inlet of the bundle would carry the tracer from the center channels to the outer channels much faster than could be done by turbulent mixing alone. The net result is that the amount of turbulent mixing could actually be less than indicated by the experimental data.

Waters[11] performed mixing experiments with a 7-rod bundle using a sodium tracer. His results for unwrapped rods indicate less mixing than found in these experiments. His result is in question, however, because the data indicated severe channeling of the flow because of eccentric positioning of the bundle within the flow housing. His chosen value of mixing for this case is conservative (low).

TWO-PHASE MIXING

Mixing during two-phase flow is very complex and not at all understood at the present time. Although it has been believed

that mixing during two-phase flow should be higher than for subcooled flow, no quantitative data have been reported. The data obtained in the present experiments represent the first such quantitative data that give a measure of mixing between rod bundle subchannels during boiling.

The values of subchannel exit enthalpy obtained from these experiments result from an integration of all mixing effects that occur along the length of the test section. If accurate values of the exit enthalpy could be measured, local values of β during boiling could be obtained, provided certain assumptions are made. Since the possible errors in the enthalpy data are significant, it is rather difficult to determine anything more than average mixing during boiling.

The average values of β during boiling were determined by trying several values of β until general agreement between calculations using COBRA and the experimental data were obtained. These calculations were done assuming that single-phase mixing existed up to the point where average bulk boiling occurred; then, a uniform value of β was used during boiling. A comparison of the calculations and experimental data in Figures 11 through 15 show that boiling improved mixing for the 0.084 in. spacings; whereas, very little improvement was noted for 0.020 in. spacing. A comparison of the selected values of average β during boiling is shown in Table III. The data show that the greatest improvement in mixing during boiling is with the larger spacing and the lower flow rate.

TABLE III. Summary of Mixing Parameter β

s, in.	$G/10^6$, lb/hr ft^2	β, Nonboiling	β, Boiling	Improvement During Boiling, %
0.084	1.0	0.006	0.024	300
0.084	2.0	0.006	0.012	100
0.084	3.0	0.006	0.012	100
0.020	2.0	0.020	0.020	0
0.020	3.0	0.020	0.020	0

A consistent variation with heat flux appears for all the measured subchannel enthalpy rises in the small channel during boiling. At the lower values of heat flux, the enthalpy rise is about what would be expected for subcooled mixing as shown in Figures 11 through 14. As boiling gets well underway along most of the channel, mixing increases by an amount greater than that found for the uniform value of mixing which would satisfy most of the boiling data. This is evident from the data tending to approach the completely mixed enthalpy rise. At the higher values of heat flux, the mixing decreases as seen by the data points being located further from the completely mixed value of enthalpy rise. This observed trend seems to be too consistent to be just experimental error. It implies that mixing during boiling is not uniform. It also appears that if the amount of mixing depends upon steam quality, a peak in mixing occurs somewhere in the low quality region. This observation suggests that the two-phase flow regime may have a significant influence upon the amount of mixing during boiling. If this is true, then parameters such as flow rate and pressure would have a significant effect on mixing during boiling.

The indication that mixing varies with steam quality and the strong effect of rod spacing on mixing during boiling rule out the extension of single-phase eddy diffusivity correlations to boiling flow. Prior to any mixing data during boiling, there was some thought given to correlating mixing during boiling on the assumption that it is proportional to the square root of a two-phase friction factor or multiplier.[6] As seen by the data from this experiment such methods are not acceptable.

PRESSURE DROP

A comparison of the predicted and measured pressure drop is shown in Figures 16 and 17. The predicted values were computed by COBRA using Koo's[12] smooth tube friction factor correlation,

$$f = 0.5\ (R_e)^{-0.32} + 0.0056 \qquad (17)$$

and the Armand[13] two-phase friction multiplier correlation presently contained in COBRA.[1]

At zero heat flux the agreement between the measured and predicted values is excellent for the 0.084 in. spacing; however, for the 0.020 in. spacing the predicted values are about 20% high. From the results of Deissler and Taylor's[14] work with turbulent flow in banks of rods, it is shown that this difference in pressure drop could be expected. Their analysis shows that the friction factor would be about 25% less for the 0.020 in. spacing as compared to the 0.084 in. spacing. Their analysis also indicates that the friction factor for the 0.084 in. spacing is about 5% lower than smooth tube data.

If the friction factor correlation was corrected to agree with subcooled pressure drop for the 0.020 in. spacing, the computed pressure drops during boiling would be consistently lower than the measured values for both spacings. This means that either the two-phase friction multiplier correlation gives low values or the two-phase void correlation is not correct, or both. The void correlation used in COBRA is the Armand[13] void correlation as modified by Massena.[15] It seems doubtful that this could be the cause of the observed differences in pressure drop, since Massena has found that the correlation agrees fairly well with the results of several investigators. It is believed that the Armand friction multiplier correlation causes the differences between the measured and computed pressure drop. The data indicates that ratio of two-phase to single-phase pressure drop is about 25% higher than that predicted using the Armand correlation.

SUBCHANNEL FLOW RATES

Measured and predicted subchannel flow rates are illustrated in Figures 5 through 15. Excellent agreement between the observed and predicted values can be seen for the 0.084 in.

spacing. Some of the variations that do exist can be attributed to small differences between the experimental conditions.

One effect that is not presently accounted for in COBRA is that of subcooled voids. Subcooled voids cause a slight reduction in the small channel flow rate prior to bulk boiling, thus causing a higher rate of enthalpy rise. This would cause the small channel to boil earlier than predicted by COBRA; therefore, the small subchannel flow rate drops before the predicted value as shown in Figures 5 through 10.

The measured flow split for the 0.020 in. spacing was about 10% greater than the predicted values as seen in Figures 8, 9, 10, 14, and 15. The probable cause of this difference is the pressure recovery at the transition from the 0.020 to the 0.080 in. spacing at the end of the test section. The area of each channel increases linearly over the last 2 in. of the test section; however, the ratio of the large channel area to the small channel area decreases about 5% because of slight dimensional differences. For pressures to maintain themselves equally during the recovery, the change in area ratio requires that a small amount of flow must be diverted from the small channel. The reported values of mass velocity could, therefore, be low for the smaller channel and high for the larger channel when the flow areas for the 0.020 in. spacing are used. The 5% change in the area ratio causes about a 10% change in the mass velocity ratio, which means that the actual subchannel mass velocities are probably in better agreement with the predicted values than shown in the figures.

TRANSVERSE CROSS FLOW RESISTANCE

Transverse crossflow resistance has been identified[1] as a weak parameter and should not cause significant subchannel pressure differences except for very closely spaced rods.

For the COBRA calculations shown in this report, the frictional constant value of f_x = 0.001 ft was used and these calculations revealed that pressure differences were generally less than 0.01 psi. The experimental data, however, show changes in the cross-channel pressure drop of about 0.05 psi for some cases during boiling. Since the pressure differences without boiling were not exactly zero, it is difficult to conclude that the increased pressure differences during boiling are real. It is possible that imperfect pressure taps could produce higher pressure differences at the higher velocities during two-phase flow. It can still be concluded, however, that the subchannel pressures are nearly equal, and that the resistance to diversion crossflow is not large, even for a 0.020 in. spacing.

INTERFACIAL SHEAR

Shear stress between adjacent subchannels is another small effect for most rod bundle designs. This is confirmed by the measured flow splits for the test section with the 0.084 in. spacing. If interfacial shear was present, then the subchannel velocities would tend to equalize as the average velocity increased. Computed flow splits for the 0.084 in. spacing, with and without interfacial shear, are compared in Table IV. Also shown are the flow splits from Figure 18 for zero pressure difference at the end of the test section. A comparison of the values shows that interfacial shear effect is small.

TABLE IV. Effect of Interfacial Shear

Nominal Mass Velocity, 10^6 lb/hr ft^2	Mass Velocity Ratio, G_2/G_1		
	Experimental	Computed[a] with COBRA $f_T = 0$	Computed[a] with COBRA $f_T = 1.0$
1.0	1.37	1.34	1.29
2.0	1.36	1.34	1.28
3.0	1.34	1.34	1.28

(a) $f_T = 0$ implies no interfacial shear; $f_T = 1.0$ implies interfacial shear using the one-dimensional approximations in COBRA.

ACKNOWLEDGMENTS

Special appreciation is given to V. R. Hill for his design of the test section and experimental layout and to K. D. Hinkle for his assembly of the test section.

REFERENCES

1. D. S. Rowe. Cross-Flow Mixing Between Parallel Flow Channels During Boiling, Part I, COBRA-Computer Program for Coolant Boiling in Rod Arrays, BNWL-371, Pt 1. Pacific Northwest Laboratory, Richland, Washington. March 1967.

2. J. M. Batch, K. G. Toyoda, and H. E. Hanthorn. The Thermal and Hydraulic Laboratory at Hanford, HW-65722 REV. General Electric, Richland, Washington. 1961.

3. M. Reichardt. "Complete Representation of Turbulent Velocity Distribution in Smooth Pipe," Zeitschrift fiir Angewandte Mathematik und Mechanik, vol. 31, p. 208. 1951.

4. S. Levy. "Turbulent Flow in An Annulus," Journal of Heat Transfer, vol. 89, series C, no. 1, pp. 25-31. 1967.

5. N. Kattchee and W. C. Reynolds. HECTIC-II - An IBM 7090 Fortran Computer Program for Heat Transfer Analysis of Gas or Liquid-Cooled Reactor Passages, IDO 28595 REV. Aerojet-General Nucleonics, San Ramon, California. December 1962.

6. S. Levy. "Fluid Flow in Nuclear Reactors." Prepared as a Contribution to Project SIFTOR, Chapter 14. August 30, 1963.

7. W. H. Bell and B. W. LeTourneau. Experimental Measurements of Mixing in Parallel Flow Rod Bundles, WAPD-TH-381. Westinghouse Electric Corporation, Bettis Atomic Power Laboratory, Pittsburgh, Pennsylvania. February 1958.

8. P. A. Nelson, A. A. Bishop, and L. S. Tong. Mixing in Flow Parallel to Rod Bundles Having a Square Lattice, WCAP-1607. Westinghouse Electric Corporation, Atomic Power Department, Pittsburgh, Pennsylvania. July 1960.

9. R. E. Grimble and W. H. Bell. An Analysis of Mixing in Parallel Flow Rod Bundles, WAPD-TH-178. Westinghouse Electric Corporation, Atomic Power Department, Pittsburgh, Pennsylvania. Undated.

10. A. A. Bishop, P. A. Nelson, and E. A. McCabe, Jr. Thermal and Hydraulic Design of the CVTR Fuel Assemblies, Westinghouse Electric Corporation, Atomic Power Division, Pittsburgh, Pennsylvania. June 1962.

11. E. D. Waters. Fluid Mixing Experiments with a Wire-Wrapped 7-Rod Bundle Fuel Assembly, HW-70178 REV. General Electric, Richland, Washington. November 1963.

12. J. P. Waggener. "Friction Factors for Pressure Drop Calculations," Nucleonics, vol 19, p. 145. 1961.

13. A. A. Armand. "The Resistance During the Movement of a Two-Phase System in Horizontal Pipes," AERE Trans. 828, 1, pp. 16-23. Izvestiya Vsesojuznogo Teplotekhnicheskogo Instituta, 1946.

14. R. G. Deissler and M. F. Taylor. Analysis of Axial Turbulent Flow and Heat Transfer Through Banks of Rods or Tubes, TID-7529 pt 1, book 2. 1956.

15. W. A. Massena. Steam-Water Pressure Drop and Critical Discharge Flow - A Digital Computer Program, HW-65706. General Electric, Richland, Washington. June 17, 1960.

NOMENCLATURE*

A = cross-sectional area, L^2

D = hydraulic diameter, L

R_e = Reynolds number, dimensionless

X = quality, $m_g/(m_g + m_f)$, dimensionless

f = friction factor based on all-liquid flow, dimensionless

$f\ell$ = diversion crossflow resistance parameter, L

g_c = gravitational constant, ML/FT^2

h = enthalpy, $XH_g + (1-X)\ h_f$, H/M

h_g, h_f = saturated vapor and liquid enthalpy, H/M

ℓ = length, L

m = mass flow rate, $Au_f\left[\rho_g \alpha\gamma + \rho_f\ (1-\alpha)\right]$, M/T

p = pressure, F/L^2

P = wetted perimeter, L

q' = heat addition per unit length, H/L

s = rod spacing, L

u = channel velocity, L/T

w = diversion crossflow between adjacent subchannels, M/TL

w' = turbulent (fluctuating) crossflow between adjacent subchannels, M/TL

X = quality, dimensionless

β = turbulent mixing parameter, dimensionless

---

* *Dimensions are denoted by:*

L = length, T = time, M = mass, θ = temperature, F = ML/T^2 = force and H = ML^2/T^2 = energy.

ε_q = eddy diffusivity for heat, L^2/T

ε_t = turbulent diffusivity for momentum, L^2/T

ρ = density, $\rho_g\alpha + \rho_f(1-\alpha)$, M/L^3

ρ_g, ρ_f = saturated vapor and liquid density, M/L^3

τ_ω = wall shear stress, F/L^2

APPENDIX A

ERROR ANALYSIS

APPENDIX A

ERROR ANALYSIS

DATA AND ACCURACY

Flow

Flow was recorded in ma and converted to mass flow rate using calibration curves and the proper fluid density. The reading and conversion could produce flow accuracy within ±1% quite easily. With the frequent calibration checks, careful reading, and consistent data reduction, flows to within ±1/2% could be realized. Although ±1/2% could be optimistic, it was assumed to be reasonable for purposes of the error analysis.

In some runs a consistent error was found in some of the flow readings. Data reduced by using these flows, gave plots of subchannel exit enthalpy versus heat flux that were of expected slope but did not intersect the proper value at zero power. Such errors can be caused by a slight obstruction in turbine flow meters. Data of this type was corrected by a constant multiplier with an error estimated at about ±1%. The different sized error bars in the data plots reflect such handling of the raw data.

Water Temperatures

Millivolt readings from thermocouples were converted to temperature using a standard calibration. Purchase specifications for the thermocouples required accuracy to within ±4 °F of the standard calibration. All thermocouples were better than this and "inplace" calibration was performed to improve accuracy. During isothermal runs, considerable temperature data were taken over a wide range of flow rates. Plots of the thermocouple temperature minus a measured reference temperature, versus the reciprocal of the flow rate at a given system

temperature were made. A linear curve was drawn through these points and the intersection with the temperature axis gave the thermocouple correction at that temperature. Correction curves were then determined. The above procedure improved the temperature measurement to about ±1 °F.

The slope of the plots mentioned above also gave heat loss information. The only regions of significant heat loss were in the connecting piping at the ends of the heated section. Most of this heat was lost by conduction through the copper electrical connections. It was assumed that the heat loss could be divided equally between the two inlet and two outlet streams. The small heat loss from the heated section was included in the piping losses. Insulation and low cooling water temperature (generally less than 200 °F) in the heat exchangers provided negligible heat loss from this part of the system.

Pressure Drop

Pressure drops less than about 16 in. of Mercury were read from an inclined manometer to within 0.01 in. For those pressure drops greater than 16 in. of mercury, the reading was on a vertical mercury manometer to within 0.01 psi. Errors caused by air in the pressure tap lines should not exist because the tap lines were bled before each day's operation to remove any air. Errors from hot water or vapor in the tap lines should be negligible since small accumulators, located a short horizontal distance from the pressure tap, condensed vapor and held any hot water drawn during "valving-in" of the manometers. Unknown errors caused by imperfect pressure tap holes could exist but should be small, especially for the axial pressure drop.

Some error in the transverse pressure drop was consistently noticed and would represent a bias on those readings that indicated a change at a particular test section flow rate. Careful inspection of the tap holes prior to assembly revealed no burns or imperfections.

CUMULATIVE ERRORS

The errors in the raw data for temperature and flow combine in various ways during data reduction. This is especially true for determining the exit enthalpy from the test section since many temperatures and flows are involved in these calculations. In order to estimate these errors that could exist in the reported data, an error analysis was carried out assuming all errors are additive. While this may be a pessimistic approach, it gives the relative errors between various sets of data. Such an approach explains the larger scatter of data for those runs where indirect flow measurement was required.

Flow Errors

Flows were measured directly with the errors taken to be 1/2% or

$$\frac{\Delta m}{m} = 0.005 \quad . \tag{A-1}$$

In some cases flows had to be obtained by subtraction. In these cases

$$m_1 = m_3 - m_2 \tag{A-2}$$

or

$$dm_1 = dm_3 + dm_2 \tag{A-3}$$

where we take the positive sign to obtain the maximum. Equations (A-2) and (A-3) may be combined to give

$$\frac{\Delta m_1}{m_1} = \frac{m_3}{m_1}\left(\frac{\Delta m_3}{m_3}\right) + \frac{m_2}{m_1}\left(\frac{\Delta m_2}{m_2}\right) \quad . \tag{A-4}$$

Equation (A-4) shows how a large error in m_1 can result if m_3 and m_2 are large compared to m_1. In some cases the flows were corrected by a constant multiple

$$m_1 = Km \quad . \tag{A-5}$$

The differential gives

$$dm_1 = Kdm + mdK \tag{A-6}$$

or

$$\frac{\Delta m_1}{m_1} = \frac{\Delta m}{m} + \frac{\Delta K}{K} \quad . \tag{A-7}$$

It was assummed that the error in K was ±1% or

$$\frac{\Delta k}{K} = 0.01 \quad . \tag{A-8}$$

Test Section Exit Enthalpy Errors

The subchannel enthalpy leaving the exit of the test section was determined from a heat balance on the heat exchanger. The heat balance gives the test section exit enthalpy as

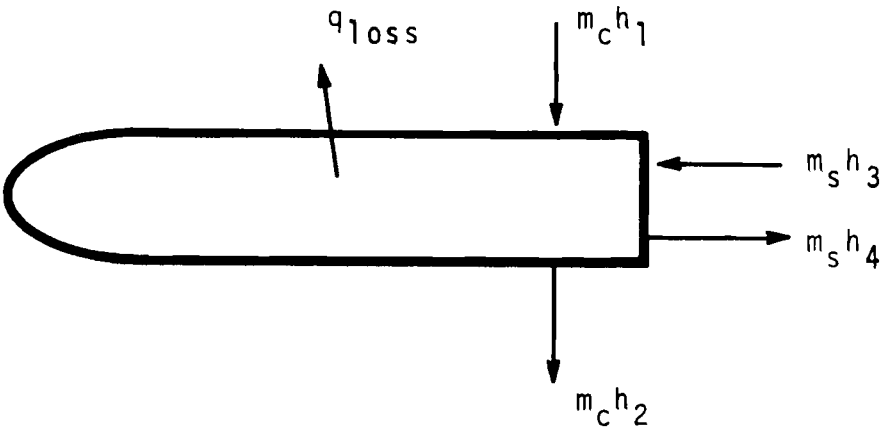

$$h_3 = h_4 + \frac{m_c}{m_s}(h_2 - h_1) + \frac{q_{loss}}{m_s} \quad . \tag{A-9}$$

Taking differentials (all positive) gives

$$dh_3 = dh_4 + \frac{m_c}{m_s}(dh_2 + dh_1) + (h_2 - h_1)\frac{dm_c}{m_s}$$

$$+ \frac{dq_{loss}}{m_s} + \left[\frac{m_c}{m_s^2}(h_2 - h_1) + \frac{q_{loss}}{m_s^2}\right] dm_s \tag{A-10}$$

or for small values of the differentials the total error in enthalpy (Δh_3) is

$$\Delta h_3 = \Delta h_4 + \frac{m_c}{m_s}\left[\Delta h_2 + \Delta h_1 + (h_2 - h_1)\left(\frac{\Delta m_c}{m_c} + \frac{\Delta m_s}{m_s}\right)\right]$$

$$+ \frac{q_{loss}}{m_s}\left[\frac{\Delta m_s}{m_s} + \frac{\Delta q_{loss}}{q_{loss}}\right] \quad . \qquad \text{(A-11)}$$

For computations a value of $\Delta h = 1.0$ Btu/lb was used for all directly measured temperatures. The relative heat loss error was assumed to be ±10% or

$$\frac{\Delta q_{loss}}{q_{loss}} = 0.1 \quad . \qquad \text{(A-12)}$$

For the cases where flows were obtained indirectly, the value of $\Delta m_s/m_s$ or $\Delta m_c/m_c$ were obtained from Equations (A-4) of (A-7).

APPENDIX B

TABULATION OF EXPERIMENTAL DATA

TABLE V. Summary of Experimental Results

Run	Spacing, In.	Heat Flux, 10^6 Btu/hr-ft^2	Mass Vel., 10^6 lb/hr-ft^2	Inlet Enthalpy, Btu/lb	Subchannel Exit Enthalpy, Btu/lb				Subchannel Mass Vel., 10^6 lb/hr-ft^2		Pressure, psia	Axial ΔP, psi	Cross Channel ΔP, psi		
					Channel 1		Channel 2								
					HX	T/C	HX	T/C	Ch. 1	Ch.2			(A)	(B)	(C)
25	0.084	0.000	2.94	300	(a)	301	(a)	299	2.40	3.21	923	5.68	0.03	0.04	-0.05
26	0.084	0.207	2.95	301	(a)	368	(a)	341	2.42	3.19	924	5.62	0.01	0.04	-0.05
27	0.084	0.331	2.96	300	(a)	406	(a)	363	2.42	3.22	923	5.66	0.01	0.04	-0.05
28	0.084	0.437	2.95	300	(a)	441	(a)	385	2.42	3.24	923	5.63	0.01	0.04	-0.05
29	0.084	0.529	2.95	298	(a)	471	(a)	402	2.42	3.21	923	5.61	0.00	0.04	-0.05
30	0.084	0.625	2.95	297	(a)	505	(a)	421	2.32	3.22	923	5.68	0.00	0.04	-0.00
31	0.084	0.679	3.00	299	(a)	(b)	(a)	(b)	1.79	3.36	913	6.05	0.05	0.05	-0.03
32	0.084	0.003	1.95	296	(a)	298	(a)	296	1.58	2.11	917	3.71	-0.02	0.02	-0.03
33	0.084	0.203	1.95	296	(a)	398	(a)	357	1.56	2.13	918	3.73	0.00	0.01	-0.02
34	0.084	0.329	1.95	295	(a)	459	(a)	393	1.56	2.11	918	3.69	0.00	0.01	-0.02
35	0.084	0.431	1.96	292	(a)	511	(a)	420	1.47	2.16	917	3.77	0.01	0.01	-0.01
36	0.084	0.476	1.99	297	(a)	(c)	(a)	442	1.09	2.19	911	3.92	0.00	0.01	-0.01
37	0.084	0.053	1.98	492	(a)	524	(a)	510	1.60	2.15	913	3.65	0.00	0.01	-0.02
38	0.084	0.101	2.00	490	(a)	(c)	(a)	522	1.30	2.24	911	3.86	0.02	0.01	-0.04
39	0.084	0.000	0.97	301	(a)	297	(a)	299	0.68	1.02	922	2.51	0.00	0.00	0.00
40	0.084	0.048	0.98	296	(a)	339	(a)	325	0.67	1.01	922	2.49	0.01	0.00	0.00
41	0.084	0.106	0.97	298	(a)	(d)	(a)	362	0.67	1.00	923	2.45	0.01	0.00	0.00
42	0.084	0.158	0.97	297	(a)	(d)	(a)	391	0.68	1.04	923	2.44	0.01	0.00	0.00
43	0.084	0.234	0.98	296	(a)	(d)	(a)	434	---	1.04	923	2.43	0.01	0.00	0.00
44	0.084	0.266	0.98	297	(a)	(d)	(a)	459	0.51	1.09	923	2.48	0.00	0.00	0.00
45	0.084	0.319	0.97	296	(a)	(d)	(a)	498	0.52	1.12	923	2.57	0.02	0.00	0.00

(a) *No valid heat balance data.*

(b) *No valid heat balance data because of flow oscillations.*

(c) *Boiling indicated.*

(d) *No valid temperature data.*

(A) *One-half inch downstream from end of heated section.*

(B) *Six inches upstream from end of heated section.*

(C) *Twelve inches upstream from end of heated section.*

TABLE V. (contd)

Run	Spacing, In.	Heat Flux, 10^6 Btu/ hr-ft^2	Mass Vel., 10^6 lb/ hr-ft^2	Inlet Enthalpy, Btu/lb	Subchannel Exit Enthalpy, Btu/lb Channel 1 HX	Channel 1 T/C	Channel 2 HX	Channel 2 T/C	Subchannel Mass Vel., 10^6 lb/ hr-ft^2 Ch. 1	Ch.2	Pressure, psia	Axial ΔP, psi	Cross Channel ΔP, psi (A)	(B)	(C)
70	0.084	0.000	0.97	490	490	(d)	501	498	0.75	1.04	924	2.27	0.00	0.00	-0.01
71	0.084	0.062	0.97	488	565	(d)	543	(c)	0.65	1.08	922	2.34	0.00	0.00	-0.01
72	0.084	0.149	0.97	487	603	(d)	607	(c)	0.78	1.04	926	3.35	-0.01	0.01	-0.00
73	0.084	0.244	0.96	487	667	(d)	669	(c)	0.72	1.07	922	4.64	0.03	0.02	0.00
74	0.084	0.378	0.96	487	818	(d)	740	(c)	0.63	1.11	918	6.86	0.00	0.01	-0.01
76	0.084	0.000	1.95	498	498	498	505	501	1.60	2.11	918	3.74	-0.03	0.00	0.00
77	0.084	0.062	1.93	506	534	(c)	534	526	1.48	2.11	919	3.81	-0.01	0.00	-0.04
78	0.084	0.101	1.95	501	563	(c)	539	(c)	1.28	2.22	919	4.23	0.01	0.00	-0.05
79	0.084	0.180	1.96	496	581	(c)	558	(c)	1.44	2.21	918	5.67	-0.05	0.02	-0.05
80	0.084	0.316	1.94	501	638	(c)	621	(c)	1.47	2.15	913	10.43	-0.01	0.05	-0.03
81	0.084	0.423	1.94	501	699	(c)	645	(c)	1.35	2.22	911	12.98	-0.04	0.04	-0.05
82	0.084	0.001	2.97	493	497	496	499	493	2.45	3.22	901	6.03	0.01	0.02	-0.09
83	0.084	0.101	2.95	499	532	(c)	525	518	2.33	3.22	901	6.12	-0.02	0.01	-0.09
84	0.084	0.151	2.94	501	550	(c)	536	(c)	1.90	3.36	899	7.25	0.05	0.03	-0.13
85	0.084	0.244	2.95	501	569	(c)	554	(c)	2.09	3.29	897	10.59	0.02	0.05	-0.10
86	0.084	0.378	2.95	499	606	(c)	582	(c)	2.09	3.30	892	16.07	-0.03	0.07	-0.09
87	0.084	0.467	2.93	503	651	(c)	606	(c)	2.00	3.31	887	20.08	0.02	0.07	-0.10
89	0.020	0.000	2.97	495	505	501	504	495	2.08	3.28	919	7.24	0.00	0.04	-0.05
90	0.020	0.101	2.99	498	585	(c)	526	529	1.63	3.46	917	7.83	-0.02	0.03	-0.05
91	0.020	0.180	3.00	498	617	(c)	548	(c)	1.62	3.47	913	11.25	-0.05	0.05	-0.05
92	0.020	0.319	3.01	495	727	(c)	581	(c)	1.52	3.52	905	18.79	-0.07	0.09	-0.06
93	0.020	0.378	3.00	506	732	(c)	611	(c)	1.64	3.47	902	23.08	0.01	0.06	-0.05

(c) *Boiling indicated.*

(d) *No valid temperature data.*

(A) *One-half inch downstream from end of heated section.*

(B) *Six inches upstream from end of heated section.*

(C) *Twelve inches upstream from end of heated section.*

TABLE V. (contd)

Run	Spacing, In.	Heat Flux, 10^6 Btu/ hr-ft^2	Mass Vel., 10^6 lb/ hr-ft^2	Inlet Enthalpy, Btu/lb	Subchannel Exit Enthalpy, Btu/lb Channel 1 HX	Channel 1 T/C	Channel 2 HX	Channel 2 T/C	Subchannel Mass Vel., 10^6 lb/ hr-ft^2 Ch. 1	Ch. 2	Pressure, psia	Axial ΔP, psi	Cross Channel ΔP, psi (A)	(B)	(C)
94	0.020	0.423	2.98	504	776	(c)	618	(c)	1.54	3.48	900	25.58	0.14	0.02	-0.10
95	0.020	0.470	2.99	502	804	(c)	631	(c)	1.56	3.49	897	27.78	0.04	-0.00	-0.08
96	0.020	0.000	1.99	492	496	(d)	491	495	1.40	2.22	916	4.35	0.00	0.01	-0.01
99	0.020	0.000	2.00	492	492	(d)	496	493	1.48	2.17	915	4.29	0.04	0.00	-0.01
100	0.020	0.103	1.99	494	584	(d)	545	(c)	1.10	2.30	914	5.28	0.05	0.02	-0.02
101	0.020	0.182	1.97	497	642	(d)	584	(c)	1.15	2.26	911	8.49	0.03	0.06	-0.04
102	0.020	0.244	1.99	496	689	(d)	614	(c)	1.17	2.27	908	11.03	-0.00	0.07	-0.02
103	0.020	0.316	1.99	496	767	(d)	649	(c)	1.09	2.28	904	14.18	0.01	0.06	-0.02
104	0.020	0.378	1.99	496	832	(d)	676	(c)	1.03	2.33	900	16.83	0.08	0.04	-0.04
105	0.020	0.423	2.01	495	883	(d)	689	(c)	1.04	2.36	898	18.43	0.03	0.04	-0.04
108	0.020	0.000	3.01	298	298	300	297	298	2.08	3.37	904	7.26	-0.00	0.04	-0.03
109	0.020	0.434	3.00	302	508	504	435	430	2.01	3.36	913	7.96	0.00	0.02	-0.01
110	0.020	0.479	3.00	297	533	(b)	444	440	1.77	3.45	914	8.02	-0.01	0.01	0.00
111	0.020	0.500	3.00	297	556	(b)	453	449	1.46	3.54	914	8.13	-0.01	0.04	-0.01
112	0.020	0.191	2.01	288	425	(d)	381	375	1.41	2.19	914	4.32	0.00	0.01	-0.01
113	0.020	0.253	1.98	302	479	(d)	415	418	1.39	2.19	916	4.30	0.00	0.00	-0.01
114	0.020	0.326	1.99	296	540	(d)	450	447	1.06	2.28	915	4.36	-0.00	0.01	-0.01
115	0.020	0.347	1.99	296	573	(d)	460	455	0.89	2.36	915	4.45	-0.01	0.00	-0.00
116	0.020	0.000	1.98	296	306	304	300	299	1.37	2.17	915	4.33	-0.01	0.01	-0.02
117	0.020	0.000	1.01	296	302	(d)	300	300	0.69	1.12	918	2.74	0.00	0.01	-0.01
118	0.020	0.107	1.02	296	427	(d)	387	392	0.71	1.16	917	2.69	0.00	0.00	0.00
119	0.020	0.158	1.01	299	498	(d)	439	440	0.70	1.14	917	2.62	0.00	0.00	0.00
120	0.020	0.183	1.01	298	565	(d)	465	465	0.51	1.21	917	2.66	0.00	-0.00	-0.01

(b) *No valid heat balance data because of flow oscillations.*

(c) *Boiling indicated.*

(d) *No valid temperature data.*

(A) *One-half inch downstream from end of heated section.*

(B) *Six inches upstream from end of heated section.*

(C) *Twelve inches upstream from end of heated section.*

DISTRIBUTION

No. of Copies	
268	AEC Division of Technical Information Extension
27	AEC Library, Washington Division of Reactor Development Technology Chief, HWOCR Branch Assistant Director, Plant Eng. Chief, Inst. & Cont. Br. Chief, Systems Eng. Br. Chief, Core Design Br. Chief, Fuel Fab. Br. Chief, Control Mech. Br. Asst. Dir., Reactor Tech. Chief, Fuels & Mat. Br. Chief, Reactor Phy. Br. Chief, Special Tech. Br. Asst. Dir., Nuclear Safety Asst. Dir., Program Analysis Water Projects Branch Research and Development Branch R. Feit R. M. Scroggins S. Strauch N. E. Todreas A. Van Echo Division of Safety Standards R. Impara Office of Assistant General Manager for Reactors Dr. R. C. Dalzell Office of Assistant General Counsel for Patents R. A. Anderson RDT Site Offices (4)
2	AEC, RDT Site Representative – PNL P. G. Holsted
3	AEC, Richland Operations Office C. L. Robinson R. K. Sharp Technical Library
1	Aerojet-General Nucleonics H. Jaffee

No. of Copies

1 Allis-Chalmers Manufacturing Company
Atomic Energy Division
6933 Arlington Road
P.O. Box 5976
Bethesda, Maryland 20014

W. S. Farmer

7 Argonne National Laboratory

Dr. Paul Lottes
Dr. M. Petrick
R. P. Stein
Leonard J. Koch
M. Novick
Robert E. Macherey
Dr. T. R. Bump

1 Atomic Energy Commission
Brussels Office
U. S. Mission to the European Communities
APO, New York, N. Y. 09667

2 Atomics International
P.O. Box 591, Canoga Park, California 91305

Senior Site Rep., AI-CE
Acting Senior Site Rep., AI

12 Atomic Energy of Canada Limited
Chalk River, Ontario, Canada

A. Pearson
G. A. Wikhammer
Scientific Representative Division
of International Affairs (10)

2 Atomic Energy Establishment
Winfrith, Heath, England

R. W. Bowring
W. S. Eastwood

2 Atomic Energy Research Establishment
Harwell, Berkshire, England

G. F. Hewitt
J. G. Collier (Nr. Didcot Berkshire)

3 Atomics International

David C. Fulton (2)
Donald T. Eggan

No. of Copies

2 Atomic Power Development Associates, Inc.
Alton P. Donnell

1 Babcock & Wilcox Company
Barberton, Ohio
P. B. Probert

2 Babcock and Wilcox Company
HWOCR Project Manager
Donald F. Judd

1 Baldwin-Lima-Hamilton Corporation
Industrial Equipment Division
Eddyston, Pennsylvania
Philip Otten

3 Brookhaven National Laboratory
Dr. O. E. Dwyer
Dr. David Gurinsky (2)

1 Canadian Westinghouse Co. Ltd.
P.O. Box 510
Hamilton, Ontario, Canada
F. Stern

2 Chicago Operations Office
G. H. Lee
Richard J. Gariboldi

1 Columbia University
Department of Chemical Engineering

4 Combustion Engineering, Inc.
HPO, Windsor Representative
F. Bevilacqua
Senior Site Representative
R. C. Noyes

4 Douglas United Nuclear, Inc.
H. R. Kosmata
P. A. Carlson
R. H. Shoemaker
T. W. Ambrose

No. of Copies

1 Duke Power Company
P. O. Box 2178
Charlotte, North Carolina 28201

E. C. Fiss

4 duPont Company, Aiken

G. Dessauar
Supervisor, Technical Information Service (2)
Site Representative, SR

2 duPont Company, Wilmington

Director, Reactor Engineering Section
J. S. Neill

1 Dynatech Corporation
17 Tudor Street
Cambridge, Massachusetts 02139

A. Bergles

18 European Contractors

AEG-Kernenergieversuchsanlage
8752 Grobwelzheim (Unterfranken)
Germany

Dr. Kirchenmayer (1)

Alshtom
38 Avenue Kleber
Paris 16e, France

M. P. Domenjoud (1)

ANSALDO
Direzione Generale (1)
Piazza Carignano 2
Genova, Italy

CEN Saclay
Boite Postale 2
Gif-Sur-Yvette (S et O), France

G. Vendryes (10)

Centre d'Etudes Nucleaires
Chemi des Martyrs
Grenoble (Isere)
France

M. Mondin (1)

No. of Copies

MAN
Abholfach
Nurnberg 2, Germany

Dr. Mayinger (1)

Reactor Centrum Nederland
112 Scheveningseweg
's gravenhage
Netherlands

Prof. Dr. M. Bogaardt (1)

SNECMA
Division Atomique
22, Quai Gallineni
Suresnes (Seine)
France

M. Fouré (1)

Technical Hogeschool Eindhoven
P. O. Box 313
Eindhoven
Netherlands

Prof. D. M. Bogaardt (1)

1 General Atomics
P. O. Box 608
San Diego 12, California

Division of General Dynamics Corp.
Dr. Peter Fortescue

1 General Electric Company, San Jose (Trumbull)
Advanced Engineering

Karl P. Cohen

3 General Electric Company, San Jose

Dr. S. Levey (2)
Earl Janssen

1 Georgia Institute of Technology

James Rust

No. of Copies	
1	Geoscience, Ltd. La Jolla, California Dr. H. F. Poppendiek
1	M. W. Kellogg Company 711 3rd Avenue New York 17, New York B. W. Jesser
1	Knolls Atomic Power Laboratory General Electric Company Schenectady, New York G. H. Halsey
2	Los Alamos Scientific Laboratory Dr. David B. Hall
2	Massachusetts Institute of Technology Dr. W. Rohsenow Dr. P. Griffith
1	MSA Research Corporation Marketing Division Callery, Pennsylvania 14024 C. H. Staub
6	NASA Lewis Research Center Librarian (3) R. Weltmann (SEPO) (2) J. M. Savino
1	New York Operations Office Jules Wise
1	North Carolina State University Dr. J. K. Ferrell
1	Nuclear Materials & Equipment Corp. Zalman M. Shapiro
1	NUS Corporation Idaho Falls, Idaho G. A. Freund

No. of Copies	
1	Oregon State University J. G. Knudsen
1	Power Reactor Development Company 1911 First Street Detroit, Michigan 48226 Arthur S. Griswold
1	Purdue University Mechanical Engineering Department R. J. Grosh
1	Rutgers, University R. L. Peskin
1	Southwest Atomic Energy Associates Post Office Box 1106 Shreveport, Louisiana 71102 J. Robert Welsh
1	Stanford University Dr. G. Leppert
1	TWR Space Technology Laboratories TRW Systems Group S. M. Zivi
2	Union Carbide Corporation (ORNL) Dr. Floyd L. Culler (2)
2	Union Carbide Corp (ORAL-Y-12) H. W. Hoffman W. R. Gambill
2	United Nuclear Corporation P.O. Box 1583 365 Winchester Avenue New Haven 4, Connecticut Alfred Strasser
2	University of Michigan (VESIAC) Dept. of Chemical and Met. Engineering J. A. Clark R. Balzhiser

No. of Copies

1 University of Minnesota
Department of Chemical Engineering
Minneapolis, Minnesota 55455

H. S. Isbin

1 University of Washington

R. W. Moulton
C. J. Kippenhan

1 Westinghouse Bettis Atomic Power Laboratory

S. Green

2 Westinghouse Electric Corporation

L. S. Tong

1 Washington State University

Dr. John Lienhard

89 Battelle-Northwest

F. W. Albaugh
R. T. Allemann
J. K. Anderson
C. W. Angle
E. R. Astley
J. M. Batch
A. L. Bement
J. J. Cadwell
P. D. Cohn
D. L. Condotta
R. F. Corlett
G. M. Dalen
R. L. Dillon
E. A. Eschbach
J. R. Fishbaugher
D. E. Fitzsimmons
G. L. Fox
J. C. Fox
M. D. Freshley
S. Goldsmith
H. E. Hanthorn
R. A. Harvey
G. M. Hesson

No. of
Copies

Battelle-Northwest (contd)

B. M. Johnson/G. Jansen
R. L. Junkins
C. E. Leach
W. R. Lewis
M. K. Millhollen
A. Padilla
L. T. Pederson
R. E. Peterson
R. H. Purcell
W. D. Richmond
T. C. Riehman
W. E. Roake
G. J. Rogers
D. S. Rowe (30)
R. I. Smith
A. M. Sutey
W. L. Thorne
R. E. Turley
P. C. Walkup
R. G. Wheeler
N. G. Wittenbrock
J. R. Worden
J. M. Yatabe
F. R. Zaloudek
Director, Heavy Water Program Office
H. Harty (6)
Technical Information Files (5)
Technical Publications (2)